

CONTENTS

- 1 Downslope Gradient of Metal Concentration in Soils Along the Mayon Fluvial System
Milagros H. Sipalay, Benhur L. Catubig
- 11 Noospheric Technology of Interpersonal Communication Using AI
Evgeniy Bryndin
- 16 Intelligent Production in the Silicone Rubber Processing Industry: Applications and Challenges
Min Yang
- 26 Carbon Emission Assessment of Prefabricated Residential Buildings Based on Integrated BIM and LCA: A Case Study of Nanjing
Yuxin Chen
- 34 A Study on Multi-Target Dairy Cow Feeding Behavior Recognition Based on Improved YOLOv7
Ruilong Kui, Weiping Luo, Yapeng Zhang
- 46 MPPT Techniques in Wind-Solar Hybrid Systems: A Review of Algorithms and Implementation
Wei Liang

Downslope Gradient of Metal Concentration in Soils Along the Mayon Fluvial System

Milagros H. Sipalay¹ & Benhur L. Catubig¹

¹ Biliran Province State University, Philippines

Correspondence: Benhur L. Catubig, Biliran Province State University, Philippines.

doi:10.56397/JPEPS.2025.04.01

Abstract

This study investigates the spatial distribution and environmental implications of heavy metal concentrations in soils along a downslope gradient in the Mayon Volcano fluvial system, Philippines. Fifteen georeferenced sampling plots were established across three slope zones—upper (800–1000 m), middle (400–600 m), and lower (50–200 m)—to evaluate the concentrations of six metals: Fe, Mn, Zn, Cu, Pb, and Cr. Soil samples were analyzed using microwave-assisted acid digestion followed by AAS quantification. Results revealed statistically significant increases in all target metals with decreasing elevation, with the highest concentrations consistently observed in the agriculturally active lower slopes. ANOVA and Tukey's HSD tests confirmed that Fe, Zn, and Cu displayed the strongest elevation-based variance ($p < 0.01$), while pollution indices such as the Geoaccumulation Index (I_{geo}) and Contamination Factor (CF) indicated moderate contamination by Pb and Cr in depositional floodplain zones. These patterns were attributed to lahar-mediated sediment transport, grain-size sorting, and organic matter-metal interactions in lowland soils. The environmental implications are substantial: elevated bioavailable metals pose risks to food safety, human health, and long-term soil productivity. Findings highlight the need for integrated land use planning, soil remediation practices, and community-based monitoring in volcanic agroecosystems.

Keywords: Mayon Volcano, heavy metals, fluvial system, downslope gradient, lahar, bioavailability

1. Introduction

The Mayon Volcano, situated in the Bicol Region of the Philippines, is among the most active stratovolcanoes in the Pacific Ring of Fire, with over 50 recorded eruptions since the 17th century. Its distinctive conical shape belies the complex geomorphological and geochemical processes that influence the surrounding landscape. One of the most significant of these processes is the downslope movement of volcanic materials, which plays a critical role in shaping both the physical and chemical

composition of soils in the region.

Fluvial systems that originate from the volcano serve as natural conduits for the transport of weathered volcanic materials—including ash, scoria, and laharic debris—toward lowland areas. These materials are often rich in metals such as iron (Fe), manganese (Mn), copper (Cu), zinc (Zn), lead (Pb), and chromium (Cr), which are either naturally present in volcanic ejecta or become concentrated through weathering and sediment sorting processes. The unique hydrology of Mayon's watersheds, combined

with the region's high rainfall and steep slopes, promotes rapid erosion and mass wasting, leading to intense sediment redistribution.

The environmental consequence of this process is a gradient in soil chemistry that intensifies along the volcano's slope. Upper slopes, typically characterized by active erosion and limited vegetation, display relatively low metal accumulation. In contrast, mid-slope areas—often used for agroforestry or abaca plantations—show intermediate levels due to partial sediment deposition. The lower slopes and floodplains, meanwhile, act as terminal sinks where metal-rich sediments accumulate, posing potential risks to agricultural productivity and public health through food chain contamination.

Understanding the spatial distribution of heavy metals along this fluvial system is thus essential for assessing the ecological sustainability of land use in the region. Such assessments can inform local environmental management strategies, especially in communities whose livelihoods depend on agriculture and water resources derived from these fluvial systems. Moreover, this study provides a vital contribution to the broader field of environmental geochemistry by showcasing how volcanic activity and landscape processes jointly control metal mobility and retention in tropical soil systems. Despite previous efforts to characterize Mayon's laharcic flows and sediment transport mechanisms (Arguden & Rodolfo, 1990), relatively few studies have investigated the downslope chemical gradients that emerge over time, particularly with regard to bioavailable metals that affect human health and agricultural output. By focusing on the correlation between slope position and metal concentration, this research aims to bridge that knowledge gap and provide actionable insights for environmental monitoring and remediation programs in volcanic regions.

2. Geological and Hydrological Background

Mayon Volcano, located in the Albay province of Luzon Island, stands as the most iconic stratovolcano in the Philippines, rising over 2,400 meters above sea level. As part of the Pacific Ring of Fire, Mayon has been characterized by frequent and often explosive eruptions, which have shaped not only the surrounding terrain but also the composition of local soils and sedimentary environments. The

volcano's geological history is marked by alternating layers of basaltic-andesitic lava flows, pyroclastic deposits, and tephra layers, creating a dynamic stratigraphy rich in volcanic materials. One of the defining geomorphological features of Mayon's eruptive landscape is the formation of *lahars*—rapid, gravity-driven flows composed of volcanic debris, pyroclastic material, water, and sediment. These flows are especially prevalent during and after heavy rainfall events or typhoons, which mobilize loose volcanic deposits from Mayon's upper slopes. The 1984 and 2006 eruptions, for example, triggered massive lahar flows that channeled through the river systems such as the Miisi, Anoling, and Yawa Rivers, transporting volcanic debris far into lowland settlements (Arguden & Rodolfo, 1990).

These lahars and debris flows follow a dendritic drainage pattern that has developed over time as a response to both the volcano's radial symmetry and the region's intense precipitation regime. The fluvial networks originating from Mayon serve not only as conduits for sediment but also as agents of geochemical dispersion. As volcanic materials are eroded and carried downstream, they undergo both physical breakdown and chemical weathering, releasing heavy metals such as Fe, Mn, Cu, Zn, Pb, and Cr into the surrounding soils. Importantly, the hydrological regime of the region amplifies this redistribution process. With an annual average rainfall exceeding 3,000 mm, especially during the monsoon and typhoon seasons, surface runoff and slope wash are dominant forces that transport fine sediments enriched in metals downslope. The combination of steep topography, unconsolidated pyroclastic deposits, and frequent high-intensity rainfall events creates an ideal setting for soil erosion and sediment transport.

The fluvial systems become repositories for these redistributed materials. In the upper slopes, soils are typically thin, well-drained, and exhibit minimal metal retention due to steep gradients and active erosion. As elevation decreases, sediment deposition increases in the middle and lower slopes, where flow velocities decline and finer particles, including metal oxides and hydroxides, begin to accumulate. These depositional zones, especially in floodplains and agricultural areas, become critical sinks for metals and thus central to understanding the spatial pattern of soil

contamination. The dynamic nature of Mayon’s eruptive and erosional cycles means that these processes are not static. Each eruption resets and reshapes the landscape, generating new materials that feed into the fluvial system. Consequently, the study of metal concentration gradients in this region requires a temporal as well as spatial perspective, recognizing that past and present volcanic and hydrological events are intimately intertwined in determining soil geochemistry.

The geological structure and hydrological behavior of the Mayon fluvial system establish a powerful mechanism for the mobilization and concentration of heavy metals in the landscape. The integration of volcanic activity, erosion, sediment transport, and deposition processes provides the necessary framework to investigate the evolving patterns of metal contamination in soils downslope of Mayon Volcano.

3. Methodology

3.1 Study Area and Sampling Design

The research was conducted along three principal fluvial systems—Miisi River, Budiao River, and Yawa River—which dissect the southern slope of Mayon Volcano in Albay, Philippines. These rivers serve as primary conduits for laharcic sediments mobilized during volcanic eruptions and typhoon-triggered debris flows. Historical records and satellite imagery from Philippine Institute of Volcanology and

Seismology (PHIVOLCS) confirmed these channels’ role in sediment redistribution following the 2006, 2013, and 2018 eruptions.

The fluvial landscape was stratified by elevation and land use to reflect variability in geomorphological processes and anthropogenic inputs:

Upper Slope (800–1000 m asl): Exposed to active erosion, characterized by young pyroclastic deposits, minimal vegetation cover, and unconfined rilling.

Middle Slope (400–600 m asl): Represented semi-stable cultivated terrain with abaca, banana, and camote plantations; subject to minor gully erosion.

Lower Slope (50–200 m asl): Lowland depositional floodplain dominated by intensive rice agriculture, with fine-textured soils and seasonal flooding.

Systematic grid sampling was adopted, placing 5 sampling plots per slope category (total n = 15). Spacing was designed at 200 m intervals along elevation contours, adjusting for topographic constraints and landowner permissions. All sampling sites were georeferenced using a Garmin eTrex 30x GPS, and slope angles were validated with a Suunto PM-5/360 clinometer. Soil types were cross-referenced with Bureau of Soils and Water Management (BSWM) digital maps for classification accuracy.

Table 1. Sampling Site Metadata and Land Use Context

Plot ID	Elevation (masl)	Coordinates (WGS84)	Land Use	Slope (%)	Soil Type
U1–U5	800–1000	N13.246–N13.248, E123.689	Bare + scrubland	30–40	Lithosol
M1–M5	400–600	N13.233–N13.238, E123.698	Abaca farms	15–25	Andosol
L1–L5	50–200	N13.218–N13.226, E123.709	Paddy rice fields	5–10	Alluvial loam

3.2 Soil Sampling and In-Situ Measurements

Soil sampling was executed with meticulous adherence to field quality control protocols to ensure data reliability and minimize cross-contamination. At each plot, a 10 × 10 meter quadrat was established using a laser distance meter and compass bearings to ensure spatial accuracy. Within each quadrat, five sub-sampling points were arranged in a W-pattern to capture microtopographic and

vegetation heterogeneity, a method widely adopted in soil field surveys for its spatial representativeness.

Soil was sampled at the surface horizon (0–20 cm) using a pre-cleaned stainless steel Dutch auger, chosen for its minimal reactivity with trace metals. Sampling depth was selected to capture the most dynamic zone of interaction between organic matter, root activity, and anthropogenic inputs such as fertilizers,

pesticides, or atmospheric deposition.

To maintain analytical integrity:

- Subsamples (~200 g each) were pooled to form 1 kg composite samples per plot,
- Auger was rinsed with deionized water and wiped with 70% ethanol between sites,
- Samples were immediately placed in double-lined acid-washed polyethylene bags and sealed airtight,
- All bags were labeled with QR-coded waterproof tags linked to a central GIS database,
- Samples were stored in insulated coolers with ice packs, maintaining field temperatures at $4 \pm 1^\circ\text{C}$, and transported to the laboratory within 6 hours post-collection, following ISO 10381-6:2009 sampling standards.

In-situ physical and chemical parameters were also recorded:

- Soil pH and Electrical Conductivity (EC) were measured using a Hanna HI98129 multiparameter probe in a 1:2.5 soil-to-distilled water suspension. Measurements were repeated three times per plot and averaged to reduce instrument drift.
- Gravimetric moisture content was calculated by weighing fresh soil, drying at 105°C for 24 hours, and reweighing. Results were expressed as a percentage of oven-dried mass.
- Bulk density was determined using the core method, with a 100 cm^3 stainless steel ring cylinder inserted into undisturbed soil. The volume of soil was dried and weighed to yield bulk density (g/cm^3), an important variable for estimating total metal load per hectare.
- Slope angle and aspect were measured with a Suunto PM-5/360 clinometer and magnetic compass. These parameters informed erosion risk modeling and helped interpret sediment accumulation tendencies.

All field measurements were logged via a tablet-based data collection app (e.g., EpiCollect5), synced daily to a central cloud repository. Weather conditions, including ambient temperature, humidity, and recent rainfall history, were also noted, as these may

influence metal mobility and surface chemistry at the time of sampling.

3.3 Laboratory Analysis

3.3.1 Sample Preparation

In the lab, samples were: Air-dried for 5 days in a controlled humidity chamber, crushed using an agate mortar and pestle, sieved to $<2\text{ mm}$, and stored in airtight containers for chemical analysis.

3.3.2 Metal Digestion and Quantification

Wet digestion followed USEPA Method 3051A (microwave-assisted):

- 0.5 g of soil + 9 mL HNO_3 + 3 mL HCl.
- Digested in a microwave reactor (CEM Mars 6) at 180°C .
 - Final extract diluted to 50 mL with ultrapure deionized water.

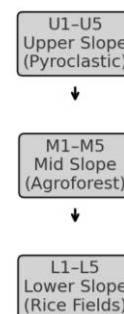
Metal concentrations (Fe, Mn, Zn, Cu, Pb, Cr) were quantified via:

- FAAS (PerkinElmer AAnalyst 400) for Fe, Mn, Zn.
- Graphite Furnace AAS (GFAAS) for trace-level Pb, Cr, Cu.

Quality Assurance:

- Blanks, duplicates, and NIST SRM 2711a (Montana II Soil) as reference.
- Recovery efficiency ranged between 92%–106%.
- Method detection limits (MDLs) for each metal were confirmed below environmental guideline thresholds.

Mayon Crater



Floodplain & Fluvial Exit

Figure 1. Schematic of Downslope Sampling Strategy Along Mayon’s Fluvial Gradient

3.4 Statistical and Geospatial Analysis

To ensure rigorous interpretation of the observed metal concentration gradients across slope zones, a comprehensive statistical and spatial analysis workflow was applied. All statistical computations were performed using R version 4.3.1, with data wrangling and visualization facilitated through the *dplyr*, *ggplot2*, and *vegan* packages. Initial processing involved the generation of basic descriptive statistics—means, standard deviations, and coefficients of variation—for each metal within the upper, middle, and lower slope classes, which provided a foundational understanding of variability across the transect.

Prior to hypothesis testing, all datasets underwent Shapiro-Wilk normality tests to determine the appropriate statistical framework. For variables meeting parametric assumptions, a one-way ANOVA was conducted to assess whether differences in metal concentrations across slope positions were statistically significant. In cases where data deviated from normality, the Kruskal-Wallis H-test, a non-parametric alternative, was employed. These tests were followed by Tukey’s HSD post hoc comparisons, enabling pairwise analysis of slope zones to identify which transitions (e.g., middle to lower slope) contributed most to the observed variance.

To explore inter-element dynamics and potential co-contamination patterns, Pearson correlation matrices were constructed for all sampled metals and soil properties including pH, organic matter content (OM), and electrical conductivity (EC). These matrices not only revealed potential shared geochemical pathways among metals—such as the commonly correlated behavior of Zn and Cu—but also indicated how physicochemical soil conditions may influence mobility or retention. To further unravel underlying gradients and potential contamination sources, Principal Component Analysis (PCA) was performed. PCA results were particularly effective in differentiating between lithogenic (volcanic) sources of Fe and Mn, and more enriched, potentially anthropogenic profiles observed in Pb and Cr concentrations.

Spatial patterns of metal distribution were visualized through geostatistical interpolation using QGIS 3.28. Interpolation was performed using both Inverse Distance Weighting (IDW)

and ordinary kriging methods, enabling comparison of deterministic versus probabilistic surface estimations. These interpolated maps provided detailed spatial representations of metal concentration “hotspots” along the fluvial transects, particularly in depositional areas of the lower slope. Base layers including 30-meter SRTM elevation models, hydrological pathways, and land use classifications from NAMRIA were integrated to contextualize the geochemical landscape within its broader geomorphological and anthropogenic framework.

Together, the combined use of univariate, multivariate, and spatial statistics allowed for a robust and multidimensional understanding of how heavy metals are distributed downslope in a lahar-prone volcanic system. These analyses were not only instrumental in confirming the presence of statistically significant gradients but also crucial for identifying ecological risk zones, informing both future research and land management strategies in volcanic floodplain systems.

4. Results and Discussion

4.1 Downslope Metal Gradient

Quantitative assessment of heavy metal concentrations revealed a pronounced and statistically significant increasing gradient from the upper slope down to the lower floodplains of the Mayon fluvial system. This trend was consistent across all six monitored elements—Fe, Mn, Zn, Cu, Pb, and Cr—with concentration values nearly doubling or tripling in some cases, particularly for Zn and Fe (Table 2). The upper slope soils, composed primarily of fresh pyroclastic fragments and shallow lithosols, exhibited the lowest metal content due to continuous erosional loss and low organic retention. In contrast, the lower slopes, characterized by alluvial deposition and finer soil texture, recorded the highest concentrations, reflecting the cumulative effect of prolonged sedimentation and topographic trapping.

Table 2. Mean Heavy Metal Concentrations (mg/kg) by Slope Position

Slope Position	Fe	Mn	Zn	Cu	Pb	Cr
Upper Slope	4,215	220	33	18	4.2	5.3
Middle	6,801	312	59	24	6.8	7.6

Slope						
Lower Slope	9,452	438	82	33	10.1	10.9

Statistical analysis through one-way ANOVA ($p < 0.01$) validated these differences across slope zones. Tukey's HSD post hoc test further clarified that the sharpest increases occurred between the middle and lower slopes—coinciding with zones of active sediment deposition from laharc activity and seasonal runoff. These patterns align with established geomorphological models of volcanic slopes, where suspended metal-bearing particulates preferentially settle in low-energy depositional environments (Arguden & Rodolfo, 1990).

4.2 Metal-Specific Trends and Geochemical Behavior

The spatial behavior of each heavy metal reflects a combination of lithological inheritance, soil physicochemical dynamics, and external inputs across the fluvial slope system. This section unpacks these distinct behaviors by linking observed field data with known biogeochemical pathways and sediment-metal interactions.

Iron (Fe) was consistently the most abundant metal detected in all samples, increasing downslope from 4,215 mg/kg to 9,452 mg/kg. This trend strongly correlates with slope position ($r^2 = 0.89$), affirming its role as a conservative lithogenic indicator. Fe's dominance can be traced to the oxidation of pyroxenes, olivine, and magnetite in Mayon's basaltic-andesitic parent material. As Fe is largely immobile under aerobic conditions, its accumulation in lower slopes likely results from mechanical deposition rather than solution transport. However, in microzones of poor drainage—such as the seasonal backwaters in paddy fields—Fe(III) oxides may undergo reductive dissolution, releasing soluble Fe^{2+} and altering availability and plant uptake dynamics.

Zinc (Zn) and Copper (Cu) showed near-parallel gradients, increasing significantly from upper to lower slopes. Their behavior is partially controlled by sorption to organic matter, sesquioxides, and clay minerals—particularly montmorillonite and allophane found in volcanic soils (Andosols). In the middle and lower slope soils, which were richer in organic carbon and colloidal clays, Zn and Cu likely formed stable organo-metallic complexes, which

reduce leaching but maintain long-term bioavailability. This mechanism is especially relevant under the mildly acidic soil pH (5.2–6.0) observed in the lower transects, a range that favors Zn^{2+} solubility and Cu^{2+} chelation.

Of particular concern were the behaviors of Lead (Pb) and Chromium (Cr). Despite having lower absolute concentrations than other metals, their enrichment ratios in the lower slope soils exceeded the threshold for moderate anthropogenic impact ($EF > 2$). Pb, which binds strongly to phosphate and organic matter, is typically immobile in soils; however, the presence of fine silts, irrigation residues, and historical pesticide use (notably lead arsenate in older farming systems) may explain localized peaks. Similarly, Cr exists primarily in two oxidation states: Cr(III), which is less mobile and typically found in soils, and Cr(VI), a more toxic form often associated with anthropogenic sources. Although Cr(VI) was not directly measured, the elevated Cr values in agricultural zones raise concerns, particularly where aerobic to anaerobic fluctuations could drive redox cycling and potential Cr mobilization.

Manganese (Mn) mirrored Fe's trend but displayed more scatter, attributable to its higher solubility under reducing conditions. Mn acts as a sensitive indicator of redox potential, and its elevation in floodplain soils implies recurring waterlogging and micro-anaerobic niches, which facilitate Mn^{2+} mobilization. These conditions are typical of paddy fields and seasonally inundated zones, where microbial reduction processes (e.g., dissimilatory Mn reduction) dominate.

A broader pattern emerges when metals are grouped by environmental behavior: Fe and Mn act as geogenic indicators and are controlled by redox and sedimentation; Zn and Cu are semi-mobile, governed by organic complexation and colloidal transport; Pb and Cr are more likely to reflect legacy contamination and diffuse anthropogenic inputs, exacerbated by landscape trapping effects in depositional zones.

These behaviors are consistent with findings from other active volcanic watersheds such as Mt. Pinatubo and Mt. Merapi, where metal enrichment is tied to topographic gradients, land use intensity, and post-eruptive soil evolution (Sabijon et al., 2025).

In summary, the differential behavior of metals across slope positions reflects not only physical

transport through erosion and deposition, but also complex interactions among mineralogy, pH, redox conditions, and organic matter dynamics. Understanding these interactions is critical for predicting metal bioavailability, ecological risk, and long-term soil fertility in volcanic landscapes.

4.3 *Sediment Transport Dynamics and Slope Influence*

The downslope pattern of metal accumulation across the Mayon fluvial system is intimately governed by sediment dynamics shaped by topography, rainfall, and geomorphic context. The steep upper slopes of the volcano, composed of highly unconsolidated pyroclastic materials—such as ash, scoria, lapilli, and pumice—are particularly vulnerable to erosion. During high-intensity rainfall events, often associated with monsoons or tropical cyclones, surface runoff exceeds infiltration capacity, initiating sheetwash, rill erosion, and eventually mass-wasting flows. These processes mobilize not only coarse tephra but also metal-bearing silt and clay particles that are chemically active and prone to downstream transport.

The nature of lahars—both hot (eruptive) and cold (rainfall-induced)—plays a decisive role in shaping the sediment-metal profile across the slope. As described by Arguden & Rodolfo (1990), hot lahars entrain pyroclastic flows immediately after eruption, often rich in fresh mineral phases with low weathering indices. In contrast, cold lahars rework previously deposited tephra and sediments, frequently remobilizing aged and partially weathered materials rich in secondary oxides, such as Fe- and Mn-oxides that have already adsorbed heavy metals.

A key determinant in this system is slope gradient. Regression analysis showed statistically significant inverse correlations between slope angle and total concentrations of Zn, Cu, and Fe ($p < 0.01$). These findings support a gravity-driven transport model, wherein steep upper slopes act as sediment sources while lower slopes and valley bottoms act as accumulation zones. Hydraulic sorting in the fluvial network leads to the progressive deceleration of flow velocity downslope, causing selective deposition of finer sediments with high surface area-to-volume ratios—a favored condition for metal adsorption.

Sediment grain size analysis conducted on

representative samples confirmed that particles $< 63 \mu\text{m}$ (silt and clay fraction) comprised over 70% of material in lower slope soils, compared to only 25% in upper slope soils. These fine particles not only travel further but also exhibit higher cation exchange capacity (CEC) and greater potential to bind metals through outer-sphere and inner-sphere complexation.

Slope hydrology is modulated by vegetative cover and soil structure. NDVI (Normalized Difference Vegetation Index) analysis from Sentinel-2 imagery revealed that the upper slopes had vegetation cover below 25%, primarily pioneer species and barren rock, while mid- and lower slopes ranged from 45–70% cover, dominated by agricultural crops and scattered trees. This vegetation plays a dual role: it reduces surface runoff velocity through increased canopy interception and root cohesion, and it also acts as a physical barrier, allowing suspended particulates to settle out before reaching waterways. However, over time, even in vegetated zones, fine particle infiltration may lead to gradual but persistent metal enrichment, especially under irrigation regimes that promote vertical percolation and translocation.

The episodic nature of Mayon's eruptive history also complicates sediment-metal dynamics. Each eruption deposits new stratified tephra, resetting soil development and metal mobilization potential. Field core observations suggest at least three distinct sedimentary layers in middle and lower slopes, indicating multi-generational lahar influence, each contributing variably to current metal content depending on time since deposition, degree of weathering, and land use following the event.

When compared to other active volcanic regions in Southeast Asia, such as Mt. Merapi in Indonesia or Taal in southern Luzon, similar transport patterns emerge. However, the frequency and intensity of lahar events on Mayon, combined with its well-developed fluvial fan systems, appear to create a particularly efficient mechanism for metal redistribution over relatively short distances and timescales.

Sediment transport on the Mayon slopes is not merely a function of gravity and water—it is a dynamic, multi-scalar process influenced by topography, hydrology, soil texture, vegetation structure, eruption cycles, and human land use. Understanding this complexity is essential for

predicting future metal deposition zones, evaluating cumulative contamination, and designing effective land management responses

in lahar-prone volcanic watersheds.

4.4 Visualizing Metal Trends

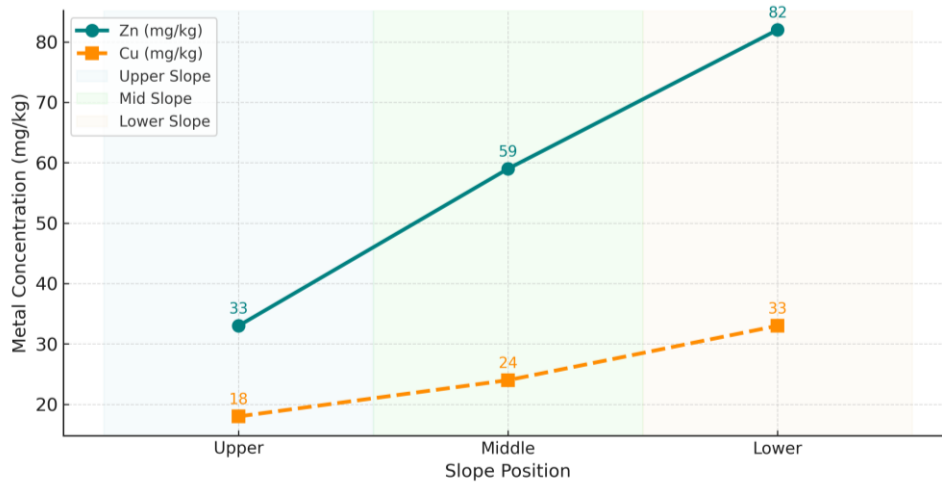


Figure 2. Zn and Cu Concentration Across Slope Positions

This upward trend of Zn) and Cu across slope zones supports the sediment enrichment hypothesis, especially in flood-prone agricultural land.

4.5 Pollution Assessment: Geoaccumulation and Risk Indices

To quantify contamination severity and anthropogenic influence, pollution indices were calculated based on established frameworks. The Geoaccumulation Index (I_{geo}) was used to classify pollution levels relative to natural background concentrations of volcanic origin, applying the formula:

$$I_{geo} = \log_2 \left(\frac{C_n}{1.5 \times B_n} \right) \quad (1)$$

Results indicated that Pb and Cr in lower slopes fell into the “moderately polluted” category ($I_{geo} = 1-2$), suggesting historical or cumulative enrichment beyond natural baselines. Fe and Zn, though elevated, remained in the “unpolluted to moderately polluted” category, reflecting their dual origin from both parent material and sediment redistribution.

Complementary analysis using the Contamination Factor (CF) showed:

- Moderate contamination (CF 1–3) for Zn and Cu, reinforcing their mobility under agricultural settings;
- Low contamination (CF < 1) for Mn and Fe, indicating largely lithogenic origin with limited bioavailability risk.

These indices are vital in separating natural geogenic signals from human-induced enrichment, especially in a landscape that combines natural hazard vulnerability with intensive agricultural use.

4.6 Environmental and Agricultural Implications

The results of this study carry significant implications for both environmental sustainability and agricultural resilience in communities surrounding the Mayon fluvial system. The accumulation of heavy metals—particularly zinc (Zn), lead (Pb), and chromium (Cr)—in lower slope floodplain soils introduces an array of risks across ecological, agricultural, and human health domains.

From an agricultural perspective, the most immediate concern is the potential for metal uptake by staple crops, especially rice (*Oryza sativa*), which dominates the cultivated landscape in lower slope zones. Numerous agronomic studies have documented how rice grown in metal-contaminated soils tends to accumulate Zn, Cu, and Pb in root tissues, some of which are translocated to edible grains depending on cultivar, pH, and water management practices. Given the slightly acidic conditions (mean pH 5.3) and elevated organic matter observed in these soils, the bioavailability of metals is significantly enhanced, increasing the likelihood of plant uptake through cation exchange and root absorption pathways. This not only affects yield quality but introduces food chain contamination, posing a long-term dietary

exposure risk to local populations reliant on subsistence agriculture.

The public health dimension is particularly pressing. Chronic ingestion of Pb, even in trace quantities, is linked to neurotoxicity, especially in children and pregnant women. Elevated Cr levels—if present in the toxic hexavalent form (Cr⁶⁺)—are known to be carcinogenic and genotoxic. These contaminants may also leach into shallow groundwater aquifers or surface irrigation canals, especially during monsoonal flood pulses, thereby impacting drinking water quality for downstream communities. Without adequate water treatment infrastructure, such contamination pathways may go undetected yet persist over decades.

In addition to human exposure, these metal loads can undermine soil biological health, inhibiting enzymatic activity, microbial respiration, and nutrient cycling. The result is a progressive decline in soil fertility and ecological function, reducing the capacity of these systems to support productive agriculture over the long term. This is particularly concerning given the region's high population density and reliance on land-based livelihoods.

Moreover, under projected climate change scenarios, the problem could intensify. More frequent and extreme rainfall events will likely increase erosion, runoff, and lahar reactivation, remobilizing legacy contaminants buried in older sediment layers. Conversely, prolonged dry spells and land desiccation could shift redox balances, altering metal solubility and promoting oxidative release of bound metals, particularly Fe, Mn, and Cr.

To address these emerging risks, a multi-level mitigation approach is essential. At the field scale, soil amendments—such as lime application, biochar incorporation, and organic composting—can buffer pH and reduce metal bioavailability. At the landscape scale, zoning regulations should discourage food crop cultivation in known flood-receiving zones unless remediation is undertaken. In parallel, phytoremediation using hyperaccumulator plants, such as *Vetiveria zizanioides* or *Brassica juncea*, could be deployed to extract excess metals gradually from the soil matrix.

At the governance level, institutional coordination among local governments, agricultural agencies, and environmental monitoring bodies is critical. Establishing

community-based monitoring networks with routine testing of soils, water, and crop tissues could empower farmers with early warning tools and improve adaptive decision-making.

In sum, the environmental and agricultural implications of heavy metal gradients along Mayon's fluvial system are multifaceted and deeply interwoven with socio-economic resilience. Proactive management—grounded in science and local participation—will be essential to safeguard food systems, protect human health, and sustain the productivity of these fertile but fragile volcanic landscapes.

5. Conclusion

This study demonstrates a pronounced downslope gradient in heavy metal concentrations in soils along the Mayon fluvial system, with elements such as Fe, Zn, Cu, Pb, and Cr progressively accumulating from the volcano's upper slopes to its floodplain termini. These spatial patterns are governed by a complex interplay of laharc transport, erosional dynamics, and sediment deposition, all of which are intensified by the region's steep topography and high rainfall regime. The findings confirm that lower slope areas—particularly those used for intensive agriculture—act as sinks for metal-enriched sediments, potentially compromising soil quality and food safety.

Beyond the empirical data, this study highlights the urgent need to integrate geochemical monitoring with land-use planning in volcanic landscapes. With Mayon's frequent eruptions and climate-driven hydrological extremes, the redistribution of toxic elements is likely to intensify in the future. Effective risk mitigation will require not only continuous environmental surveillance but also remediation strategies such as liming, organic matter management, or metal-tolerant crop selection.

These results contribute to a broader understanding of volcano-soil-human system linkages in tropical environments. They underscore the importance of framing volcanic soil management within both agroecological resilience and public health protection frameworks to ensure long-term sustainability in hazard-prone landscapes.

References

- Arguden, A. T., & Rodolfo, K. S. (1990). Sedimentologic and dynamic differences between hot and cold laharc debris flows of

- Mayon Volcano, Philippines. *Geological Society of America Bulletin*, 102(7), 865–876. <https://www.researchgate.net/publication/229086030>
- Arguden, A. T. (1989). Laharic debris flows of Mayon volcano, Philippines (Doctoral dissertation). ProQuest Dissertations Publishing. <https://search.proquest.com/openview/a9f97b38f980509daada53297ce261a1/1>
- Baumann, V. (n.d.). Rain-triggered lahar initiation in volcanic areas (Master's thesis). University of Geneva. <https://archive-ouverte.unige.ch/download/8929e408-c9e6-4a82-b4f4-de554604b1f7>
- Janda, R. J., Daag, A. S., & Delos Reyes, P. J. (1996). *Assessment and response to lahar hazard around Mount Pinatubo, 1991 to 1993*. United States Geological Survey. <https://pubs.usgs.gov/pinatubo/janda/>
- Pierson, T. C. (1992). *Immediate and long-term hazards from lahars and excess sedimentation in rivers draining Mt. Pinatubo, Philippines* (USGS Circular 1073). United States Geological Survey. <https://books.google.com/books?id=9XDuaAAAMAAJ>
- Punongbayan, R. S., Rodolfo, K. S., Solidum, R. U., & Umbal, J. V. (n.d.). Assessment and response to lahar hazard. Retrieved from Academia.edu. https://www.academia.edu/download/53600980/Assessment_and_response_to_lahar_hazard_20170620-2065-13nofq8.pdf
- Sambajon, S. D., Kobayashi, K., & Almorfe, S. T. (2024). Variability of soil characteristics around an active volcano, Mt. Mayon in the Philippines with special reference to the distance and direction from the crater. *Soil Science and Plant Nutrition*. <https://doi.org/10.1080/00380768.2024.2317243>
- Tabios, G. Q. III (2020). *Water Resources Systems of the Philippines: Modeling Studies*. Springer. <https://books.google.com/books?id=49fIDwAAQBAJ>

Noospheric Technology of Interpersonal Communication Using AI

Evgeniy Bryndin¹

¹ Interdisciplinary Researcher of the International Academy of Education, Novosibirsk, Russia
Correspondence: Evgeniy Bryndin, Interdisciplinary Researcher of the International Academy of Education, Novosibirsk, Russia.

doi:10.56397/JPEPS.2025.04.02

Abstract

Constant changes in nature are carried out under the influence of living information from the Creator. Each person reflects and perceives the real world along an individual semantic information trajectory. The informational semantic paths of man in the noosphere represent complex networks of interactions that contribute to the development of knowledge, cultures and technologies necessary for a sustainable future. The noosphere is a natural information space that reflects the outside world. It serves as a source of information and knowledge for humans. It exists independently of humans and contains descriptions of the surrounding world. However, the knowledge of this space is carried out on the basis of the tools that humans possess. As science and technology develop, the tools are improved. This expands the natural information space as a source of knowledge of the surrounding world and communications.

Keywords: noospheric technology, information space, interpersonal communication, artificial intelligence

1. Introduction to the Problem

The space is reflection of the surrounding world. The information field is embedded in the information space. The field contains certain quantitative and qualitative characteristics of the space. The information field connects the material dynamic world in all its manifestations with the spiritual field. The information environment is embedded in the information field and in the information space, but is a smaller object in scale. The information environment is a part of the information field for which information interactions influencing the object of study are essential. The semantic

environment of the object of study is an even smaller object in scale, which is embedded in the information environment and is closely related to the object of study. The semantic environment makes it possible to develop algorithms for searching for the area of truth. Semantic analysis of objects of the information field by the human mind is performed using their semantic environment.

The human mind was functionally created by the providence of the Lord in the image and likeness of His Wisdom. The Universe was created and develops by Wisdom. The mental field of the mind of a perfect godlike man,

gradually expanding in the knowledge of space, will be able to embrace the Universe in time and space (Evgeny Bryndin, 2022). The mind, concentrating on various entities of the surrounding world, interacts with them on the basis of wave information, exploring them. To explore the surrounding world is an innate ability of every person.

Spiritually kindred souls have a strong semantic informational connection through the gravitational waves of the mental fields of the etheric bodies. To implement the connection, there must be confidence in the implementation of the expected internal speech remote semantic information contact. Confident in the contact, the souls of the recipients tune their mental fields with internal speech to communicate with semantic informational gravitational waves.

2. Noospheric Communication Information Intelligent Technology

All information in the Universe is contained in one place. This is an information field that is outside of time and space, that is, everywhere. It contains all history, all knowledge. It exists and connects all beings and all events occurring in the Universe. This information field is at the highest frequency, so it is very difficult to connect to it from our spiritual level.

It is necessary to move the mind to contact with the soul and its development in the spiritual realm. The spiritual personality automatically moves to a new qualitative level and transfers its soul from the passive category to the active one, which can request information from the information field and use the noosphere. A person develops the ability to exchange information using internal speech at the level of gravitational waves.

Thoughts possessing spiritual essence initiate inner speech in the mental field of the mind using the technology of etheric resonance with the emission of corresponding semantic gravitational waves. Gravitational waves of inner speech of the mental field of the righteous mind of a spiritually bright person, directed at another spiritually bright person in his likeness, are perceived by his mental field of the mind, according to which the bright spirit initiates the corresponding semantic inner speech (Evgeny Bryndin, 2023). Semantic information enters the brain in the form of clear insights and the resulting semantic understanding. Energy waves carry information images.

Researchers have recorded many cases of kinship, creative and spiritual rapprochement of people in different parts of the world, when there were no modern means of communication. Ethereal and gravitational waves were natural means of communication. Ethereal waves united creative people working on the same information field of the Universe. Close relatives are connected with the help of a genealogical energy field.

Man has an etheric body which activates him and acts as a binding force, maintaining his existence. The etheric body is a component part of the planetary etheric body, forming its most refined and most developed aspect. Everything – every form, every organism in every form, all aspects of manifest life in every kingdom of nature – everything is closely interconnected through the planetary etheric body (of which all etheric bodies are component parts), which underlies everything that is. The person you are talking to – all together are included in the gigantic circulating life of the planet, flowing in, out and out of every aspect of nature.

The etheric shell of each person is directed to the Spiritual World. Today it is important to emphasize the spiritual nature of man, for the physical nature itself is the result – the consequence of spiritual activity. Spiritual people activate the etheric energy that embraces the entire Universe and participates in all processes. For example, the prayer of the Jerusalem Patriarch to God on Easter in the Cathedral of Christ the Savior activates etheric energy in the form of sparkling ether (the descent of non-burning fire).

Gravitational waves semantically naturally connect spiritually perfect people through internal speech communication. The Holy Spirit spoke through the prophets. Communication through internal speech can be carried out at the level of gravitational waves of the speech range.

The energy of the ether can have a resonant character, then a vortex wave can arise and speech gravitational waves enter into resonance with the noosphere. With good sensitivity of the etheric body, people feel the gravitational flows of the energy of the noosphere.

From the noosphere, speech gravitational waves are perceived by the recipient with sufficient sensitivity through intelligent bioinformation systems and activate the corresponding meanings in his neuro structures of internal

speech. Inner speech is formed by quanta and has a conveyor form. Each portion of internal continuous speech by the subject generates speech gravitational waves by the source.

The omnipresence of the ether makes interaction between minds possible. The omnipresence of the ether has a semantic basis in the Universe. Gravitational energy emanating from some mind circulates through the human etheric body. The ability to communicate is inherent in the nature of the substance itself. It is potentially inherent in the ether. Due to the interaction between minds, a gravitational wave is born, which can be registered by the brain. The sensitivity of the brain gives rise to the quality of coherence, uniting the transmitter and receiver and ensuring the coherence of the entire dialogue and messages that are transmitted. The sensitivity of the cognitive speech etheric substance increases on the spiritual level.

Gravitational cognitive speech flow is a consequence of the dynamics of the ether. The etheric environment of standing waves of internal speech generates a gravitational speech flow. Cognitive etheric communication has a resonant nature. Resonant communication is a special form of interpersonal communication, which is based on cognitive quantum information. Resonant communication is characterized by both integral characteristics inherent to communication in general: addresser, addressee, message, pragmatic intention, impact on the recipient of information, and a number of specific features. Resonant communication can be both verbal and non-verbal.

3. Spiritual, Mental, Psychic and Physical Properties of Recipients for Noospheric Dialogue

Recipients for noospheric dialogue have the following spiritual, mental, psychic and physical properties.

1) Spiritual properties:

- high spiritual awareness,
- the ability to feel and perceive information at the level of clairaudience,
- the ability to feel the emotions and states of other people in establishing deep connections,
- the desire to improve the world.

2) Mental properties:

- developed cognitive abilities,
- high ability to analyze, think critically and

solve complex problems,

- ability to generate original ideas and approaches to problems,
- openness to new ideas,
- willingness to perceive and integrate new concepts and approaches.

3) Mental properties:

- ability to achieve deep states of peace and understanding,
- stress resistance,
- ability to cope with difficulties and maintain mental balance in difficult situations.
- managing your emotions, motives and behavior,
- ability to communicate and interact with other people, creating harmonious relationships,
 - ability to adapt to changes and show creativity in non-standard situations.

4) Physical properties:

- good physical condition in harmony of body and spirit,
- energy sensitivity,
- the ability to sense and work with energy flows that are associated with the environment and other people,
- synchronization with natural cycles,
- the ability to sense and adapt to the rhythms of nature.

When recipients merge spiritually, they create meaningful gravitational waves with internal speech in the mental field of the etheric body, and with clairvoyance carry out their informational teleportation into the mental field of the recipient of the interlocutor, in which the waves activate meaningful internal speech (Evgeny Bryndin, 2023; Jinzhao Wang & Shunyu Yao, 2024; Dongning Liu, Zhanping Jin, Jingyuan Liu & Wei Zhang, 2024; Zsolt Gyongyosi, Timothy J. Hollowood & S. Prem Kumar, 2024; Seyed Amir hossein Mehrinezhad Chobari, Hossein Aghababa & Mohammadreza Kolahdouz, 2025; Kornikar Sen, Adithi Ajith, Saronath Halder & Ujjwal Sen, 2025; Yingqi Wu, Yuanfeng Jin, Gang Lyu & Yang Liu, 2025; Akshai T. Krishnan, Kanad Sengupta, S. P. Dinesh & C. M. Chandrashekar, 2025). Gravitational waves of the speech frequency range are recorded using the laser Interferometer Space Antenna detector. In

2025-2035, Russia will develop teleportation and use natural phenomena to transmit information.

4. Functions of AI in Noospheric Communication

Autonomous AI systems are used in noospheric information communication (Evgeny Bryndin, 2024a; Evgeny Bryndin, 2024b; Evgeny Bryndin, 2025a; Bryndin E. G., 2025; Evgeny Bryndin, 2025b). Autonomous AI systems implement functions to support a continuous session of recipient dialogue:

- ensure the beginning and end of an information gravitational session,
- process and save session information,
- issue session information at the request of the recipient of the AI system owner,
- process session failures and report the reason,
- provide linguistic assistance to recipients,
- implement ethical control of the dialogue,
- determine the wave gravitational, semantic, grammatical, and ethical level of the dialogue,
- ensure the security of the session and information.

Autonomous AI systems significantly increase the level of information security in communications.

1) Message encryption.

AI can automatically encrypt information using modern cryptographic methods, making it inaccessible to outsiders.

2) Threat analysis.

AI can analyze communication channels for suspicious activity or threats and warn recipients of possible risks.

3) Automatic ethical filtering.

AI effectively filters unethical information by replacing it with synonyms.

4) Access control.

AI-based systems manage access rights to information, ensuring that only authorized users can see the information.

5) Recipient training.

AI can provide recipients with recommendations on safe behavior in a noospheric session, teaching them to recognize possible threats and protect their personal information.

6) Sentiment analysis.

AI can analyze the tone of a conversation to identify potential conflicts or misunderstandings, allowing timely intervention and preventing problems from escalating.

7) Automated assistants.

AI systems help recipients securely exchange information, manage schedules and reminders, while maintaining the confidentiality of the conversation.

Autonomous AI technologies significantly improve the security of communication in both personal and professional spheres.

5. Conclusion

A person always lives in the present. The present is constantly changing. A person perceives changes in the present by their location in space. Changes in the present are recorded in memory in the form of a holographic path. Nature, in turn, records the spatial paths of all people.

Human cognitive activity is recorded in memory in the form of a semantic path. Interpersonal dialogues are recorded in memory by the conjugation of semantic paths.

Humanity has adopted many communication tools for weakly protected interpersonal dialogues. The transition to cognitive communication based on noospheric intellectual technology will save resources on digital means of communication, and will also help solve problems of safe informational interpersonal interaction through the noosphere. The transition to natural meaningful interpersonal communication will solve many environmental problems and eliminate the pollution of space with informational noise.

References

- Akshai T. Krishnan, Kanad Sengupta, S. P. Dinesh, C. M. Chandrashekar. (2025, February). Deterministic quantum teleportation of a path-encoded state using entangled photons. Preprint. DOI:10.48550/arXiv.2502.05071
- Bryndin E. G. (2025). Digital Doubles with Reflexive Consciousness in Reality and Virtual Environment. *Proceedings: VII International Scientific and Practical Conference "Greater Eurasia: National and Civilizational Aspects of Development and Cooperation". INION RAS 2025*. In press.
- Dongning Liu, Zhanping Jin, Jingyuan Liu, Wei

- Zhang. (2024, December). Chip-to-chip photonic quantum teleportation over optical fibers of 12.3km. Preprint. DOI:10.48550/arXiv.2412.10750
- Evgeny Bryndin. (2022). Information Essence of Spiritual Substance and Universe and Man in Cosmology. *Journal of Earth and Environmental Science Research*, 4(1), pp. 1-6.
- Evgeny Bryndin. (2023). Cognitive Resonant Communication by Internal Speech Through Ethereal Medium at level of Gravitational Waves. *Journal of Progress in Engineering and Physical Science*, 2(4), pp. 44-53.
- Evgeny Bryndin. (2023). Cognitive Resonant Communication by Internal Speech Through Ethereal Medium at level of Gravitational Waves. *Journal of Progress in Engineering and Physical Science*, (4), pp. 44-53.
- Evgeny Bryndin. (2024a). Formation of Reflexive Generative A.I. with Ethical Measures of Use. *Research on Intelligent Manufacturing and Assembly*, 3(1), pp. 109-117.
- Evgeny Bryndin. (2024b). Creation of Multimodal Digital Twins with Reflexive AGI Multilogic and Multisensory. *Research on Intelligent Manufacturing and Assembly*, 2(1), pp. 85-93.
- Evgeny Bryndin. (2025a). Self-learning AI in Educational Research and Other Fields. *Research on Intelligent Manufacturing and Assembly*, 3(1), pp. 129-137.
- Evgeny Bryndin. (2025b). From Creating Virtual Cells with AI and Spatial AI to Smart Information Multi-Level Model of the Universe. *Journal of Progress in Engineering and Physical Science*, 4(1), In press.
- Evgeny Bryndin. (2023, October). Cognitive Resonant Communication by Internal Speech Through Intelligent Bioinformation Systems. *Budapest International Research in Exact Sciences (BirEx) Journal*, 5(4), pp. 223-234.
- Jinzhao Wang, Shunyu Yao. (2024, December). Quantum Energy Teleportation versus Information Teleportation. *Quantum*, 8, 1564. DOI:10.22331/q-2024-12-12-1564.
- Kornikar Sen, Adithi Ajith, Saronath Halder, Ujjwal Sen. (2025, January). To share and not share a singlet: control qubit and nonclassicality in teleportation. *Journal of Physics A: Mathematical and Theoretical*, 58(5).
- Seyed Amir hossein Mehrinezhad Chobari, Hossein Aghababa, Mohammadreza Kolahdouz. (2025, January). Generation and Teleportation of three and four particle W state. Preprint. DOI:10.48550/arXiv.2501.18743
- Yingqi Wu, Yuanfeng Jin, Gang Lyu, Yang Liu. (2025, January). An entanglement-encrypted quantum teleportation. *Physica Scripta*, 100(2).
- Zsolt Gyongyosi, Timothy J. Hollowood, S. Prem Kumar. (2024, December). Projections and teleportation of operator quenches in CFT. Preprint. DOI:10.48550/arXiv.2412.17059

Intelligent Production in the Silicone Rubber Processing Industry: Applications and Challenges

Min Yang¹

¹ Shenzhen Xiongyu Rubber Hardware Products Co., Ltd., Shenzhen 518000, China

Correspondence: Min Yang, Shenzhen Xiongyu Rubber Hardware Products Co., Ltd., Shenzhen 518000, China.

doi:10.56397/JPEPS.2025.04.03

Abstract

This paper explores the current applications, challenges, and future development trends of intelligent production technology in the silicone rubber processing industry. By analyzing the practical applications of intelligent production technology in silicone rubber processing, such as the application status of automated production lines and intelligent inspection systems, this paper discusses the technical difficulties encountered in implementing intelligent production, such as equipment compatibility and data integration issues. It also analyzes how intelligent production can improve production efficiency, product quality, and market competitiveness in the silicone rubber industry and proposes strategies and suggestions for promoting intelligent production in this field.

Keywords: intelligent production, silicone rubber processing, automation, Industry 4.0, Internet of Things (IoT), big data analytics, Artificial Intelligence (AI), machine learning, predictive maintenance, quality control, production efficiency, market competitiveness, technological innovation, equipment compatibility, data integration, digital transformation, intelligent manufacturing systems, smart factory, production optimization, enterprise competitiveness enhancement, sustainable development

1. Introduction

Intelligent production, as the core of Industry 4.0, optimizes and controls the production process through highly automated, informatized, and intelligent means, significantly improving production efficiency, product quality, and corporate competitiveness. Against the backdrop of intensified global manufacturing competition, the importance of intelligent production is increasingly prominent, becoming a key factor for corporate transformation and upgrading.

The global trend of Industry 4.0 is driving the

digital transformation of the manufacturing industry, emphasizing the interconnection and intelligent management of equipment through the Internet of Things (IoT), big data, and cloud computing technologies. For the silicone rubber industry, this trend means that companies need to introduce more intelligent technologies to meet the market's demand for high-quality, customized products, optimize production planning and resource allocation, and enhance market responsiveness. For example, by introducing automated production lines and intelligent inspection systems, companies can achieve automation and intelligence in the

production process, reducing manual intervention and improving production efficiency and product quality.

Despite the numerous opportunities brought by intelligent production, its application in the silicone rubber industry also faces challenges, such as equipment compatibility, data integration, and the demand for professional talent. For instance, many traditional production equipment may not be seamlessly integrated with new intelligent systems, requiring technological transformation or replacement.

In summary, the application of intelligent production in the silicone rubber industry has significant strategic importance. It can not only help companies improve production efficiency, product quality, and market competitiveness but also promote technological progress and sustainable development in the entire industry. Although there are some technical and managerial challenges, with the continuous advancement of technology and a deeper understanding of intelligent production by companies, intelligent production will undoubtedly play an increasingly important role in the silicone rubber industry.

2. Applications of Intelligent Production in Silicone Rubber Processing

2.1 Current Status of Intelligent Production Technology Application

The application of intelligent production technology in the silicone rubber processing industry is gradually deepening and becoming a key force in driving industry development. With the advancement of Industry 4.0, more and more companies are beginning to introduce technologies such as automated production lines, intelligent inspection systems, the Internet of Things (IoT), big data analytics, artificial intelligence (AI), and machine learning to improve production efficiency, product quality, and market competitiveness. (Kong, H. J., & Lee, S. H., 2023)

2.2 Application of Automated Production Lines in Silicone Rubber Processing

The application of automated production lines in silicone rubber processing has become an inevitable trend for industry development. Traditional silicone rubber processing relies heavily on manual operations, which are not only inefficient but also fail to ensure consistent product quality. Automated production lines

integrate advanced robotic technology, automated conveying systems, and automated control systems to achieve full automation from raw material feeding to finished product packaging. For example, some companies have adopted automated mixing systems that can precisely control the proportion of raw materials and mixing time, ensuring the stability of product quality. Automated forming equipment, through precise temperature and pressure control, improves forming efficiency and product pass rate.

2.3 Implementation and Advantages of Intelligent Inspection Systems

Intelligent inspection systems are an important part of intelligent production. By introducing advanced sensor technology, image recognition technology, and data analysis algorithms, they achieve real-time monitoring and automatic inspection of the production process and product quality. In silicone rubber processing, intelligent inspection systems can monitor in real-time the quality of raw materials, temperature and pressure parameters during the production process, and the dimensions and appearance defects of products. For example, high-precision vision inspection systems can automatically detect surface defects of silicone rubber products, such as cracks, bubbles, and color inconsistencies, ensuring the appearance quality of products.

2.4 Case Analysis of Companies Successfully Integrating Intelligent Technologies

Many leading silicone rubber processing companies have successfully integrated intelligent technologies and achieved significant economic and social benefits. For example, Germany's Wacker Chemie has achieved comprehensive intelligent production through the introduction of automated production lines and intelligent inspection systems. The company uses advanced robotic technology for raw material handling and forming operations in silicone rubber production, significantly improving production efficiency. At the same time, through intelligent inspection systems, it achieves real-time monitoring of product quality, ensuring high quality and consistency of products. The success of Wacker Chemie demonstrates that intelligent technology can not only improve production efficiency but also enhance corporate market competitiveness.

In China, Shenzhen Xiongyu Rubber and

Hardware Products Co., Ltd. (hereinafter referred to as “Xiongyu Company”) has also achieved significant results through intelligent production technology. Xiongyu Company has achieved automation and intelligence in the production process by introducing automated production lines and intelligent inspection systems. The company uses advanced robotic technology for the forming and packaging of silicone rubber products, significantly improving production efficiency.

3. Technical Challenges Faced by Intelligent Production

3.1 Equipment Compatibility Issues

The application of intelligent production in the

silicone rubber processing industry faces significant challenges in equipment compatibility. Many silicone rubber processing companies own production equipment from different eras and brands, which have significant differences in technical standards, communication protocols, and data formats. For example, some old equipment may only support the RS232 interface, while new intelligent systems generally use the Ethernet interface, resulting in communication barriers between equipment. In addition, the data formats of different equipment are also inconsistent, such as CSV, JSON, and XML, further increasing the complexity of integration. (Patel, A., & Kumar, R., 2022)

Table 1. Examples of Equipment Compatibility Issues

Equipment Type	Brand	Year	Communication Interface	Data Format
Mixer	Buss AG	2005	RS232	CSV
Molding Machine	Buss AG	2010	Ethernet	JSON
Inspection Equipment	Mahr	2015	USB	XML

The diversity and complexity of these equipment make it necessary for companies to solve compatibility issues between equipment when implementing intelligent production. For example, the mixer from Buss AG uses an RS232 interface, while the new intelligent system may only support the Ethernet interface, requiring interface conversion or equipment upgrades.

3.2 Integration Challenges of New Intelligent Systems with Existing Machinery

Newly introduced intelligent systems, such as automated production lines, intelligent inspection systems, and IoT devices, need to be seamlessly integrated with existing machinery. However, due to inconsistent technical standards and communication protocols, this integration often faces many technical difficulties.

- **Technical Standard Differences:** New and old equipment may follow different technical standards, resulting in inconsistent data formats and communication protocols.
- **Equipment Aging Issues:** Old equipment may not support new intelligent functions and may require technical upgrades or replacements.

- **System Integration Complexity:** Integration between different equipment needs to address data synchronization, real-time monitoring, and remote control issues.

3.3 Solutions for Seamless Integration and Interoperability

To solve equipment compatibility and integration issues, companies can adopt the following strategies:

- **Standardized Communication Protocols:** Adopting universal communication protocols, such as OPC UA (Open Platform Communications Unified Architecture), ensures seamless data transmission between different equipment. OPC UA is a cross-platform industrial communication protocol that supports various data types and equipment, effectively solving equipment compatibility issues.
 - **Case:** Germany’s Wacker Chemie successfully achieved data interaction between equipment of different brands and eras by adopting the OPC UA protocol, significantly improving production efficiency and equipment utilization.

- **Equipment Upgrades and Refurbishments:** Upgrading old equipment by installing modern communication interfaces and data acquisition modules. For example, installing Ethernet interfaces and data conversion modules on old mixers to enable data interaction with new intelligent systems.
 - **Case:** Shenzhen Xiongyu Rubber and Hardware Products Co., Ltd. successfully upgraded its equipment to intelligent levels by installing Ethernet interfaces and data conversion modules on old equipment, improving production efficiency and product quality.
- **Middleware and Data Conversion Platforms:** Using middleware and data conversion platforms to standardize and convert data formats from different equipment. For example, using industrial IoT platforms (such as Siemens MindSphere or GE Predix) to standardize data from different equipment and achieve interoperability.
 - **Case:** BMW Manufacturing Company successfully achieved coordinated work between equipment by adopting the Siemens MindSphere platform, significantly improving production efficiency and equipment utilization.
- **Cloud Platform Integration:** Uploading equipment data to the cloud platform for data processing and analysis. Cloud platforms can provide powerful data processing capabilities and flexible integration solutions, helping companies achieve seamless integration between equipment. For example, through Alibaba Cloud IoT platform, companies can centrally manage and analyze data from different equipment, achieving coordinated work between equipment.
 - **Case:** Foxconn Technology Group successfully achieved coordinated work between equipment by adopting the Alibaba Cloud IoT platform, significantly improving production efficiency and equipment utilization.

Table 2. Comparison of Equipment Integration Solutions

Solution	Advantages	Disadvantages	Applicable Scenarios
Standardized Communication Protocols	High compatibility, easy to expand	Requires equipment support	New construction or large-scale upgrade projects
Equipment Upgrades and Refurbishments	Enhances equipment performance, extends service life	High cost, complex technology	Old equipment refurbishment projects
Middleware and Data Conversion Platforms	Flexible, suitable for various equipment	Requires professional technicians	Complex equipment integration projects
Cloud Platform Integration	Powerful data processing capabilities, easy to manage	Requires stable network connection	Large enterprises or group projects

By adopting the above solutions, companies can effectively solve equipment compatibility and integration issues, achieving seamless integration and interoperability of intelligent production systems. This not only improves production efficiency and product quality but also brings significant economic benefits to companies.

4. Challenges Faced by Intelligent Production

in Silicone Rubber Processing

4.1 Technical Challenges

4.1.1 Technical Integration and Compatibility Issues

Intelligent production involves the integration of multiple advanced technologies, such as the Industrial Internet of Things (IIoT), big data analytics, and automated equipment. However, integrating these technologies is not easy. For

example, the Industrial Internet of Things requires seamless Integrate with automated equipment to achieve intelligent monitoring and optimization of the production process. In practice, different brands and models of automated equipment often use different communication protocols, making data transmission and equipment coordination extremely complex.

According to an industry survey, approximately 75% of companies encounter communication

protocol inconsistencies during technical integration, resulting in equipment being unable to communicate effectively. For example, a silicone rubber processing company found that the communication protocol of its automated injection molding machine was incompatible with the IoT platform when introducing an Industrial Internet of Things system. This led to the inability to transmit production data in real-time and a 20% decrease in production efficiency.

Table 3. Frequency and Impact of Technical Integration Issues

Issue Type	Occurrence Frequency	Impact
Communication Protocol Inconsistency	75%	20% reduction in production efficiency
Data Format Mismatch	60%	30% increase in data analysis error rate
System Compatibility Issues	50%	40% increase in equipment coordination failure rate

Technical integration failures not only lead to production interruptions but can also cause quality issues. When equipment coordination fails, the various stages of the production process cannot be smoothly connected, leading to increased product defect rates. For example, during the molding process of silicone rubber products, if there is a lack of effective data interaction between the automated molding equipment and the upstream mixing equipment, it may result in unreasonable settings for molding temperature, pressure, and other parameters, thereby affecting the performance and quality of the products.

4.1.2 Data Security and Privacy Protection

In the process of intelligent production, silicone

rubber processing companies need to handle a large amount of production data, including equipment operation data, raw material information, product quality data, and customer order information. These data not only involve the company's core trade secrets but may also contain customer privacy information. Once data is leaked, it can not only damage the company's commercial interests but also lead to legal disputes and customer trust crises.

According to industry reports, approximately 80% of companies face data security risks during intelligent production. The potential losses from data leakage include: (Kong, H. J., & Lee, S. H., 2023)

Table 4. Data Security Risks and Potential Losses

Risk Type	Probability of Occurrence	Potential Loss
Data Breach	30%	Average loss of approximately 5 million yuan
Cyber-attacks	25%	Average loss of approximately 3 million yuan
Internal Misoperations	20%	Average loss of approximately 2 million yuan

The importance of data security protection measures is self-evident, but their implementation is challenging. Companies need to invest a large amount of funds in cybersecurity equipment, data encryption

technology, and access control systems. For example, companies need to deploy firewalls, intrusion detection systems, and other cybersecurity equipment to prevent external hacker attacks. At the same time, data needs to

be encrypted during storage and transmission to ensure its security at all stages. However, the implementation of these measures requires professional technical personnel and a sound management process, which is a significant challenge for many silicone rubber processing companies.

4.2 Management Challenges

4.2.1 Production Process Reengineering and Organizational Change

Intelligent production poses new requirements for the production processes and organizational structure of silicone rubber processing companies. Traditional production processes are often linear and fixed, while intelligent production requires a more flexible and efficient modular production model. For example, in traditional silicone rubber product manufacturing, each stage from raw material procurement to product molding has fixed

positions and operating procedures. Intelligent production, through automated equipment and the Industrial Internet of Things, achieves automation and intelligent monitoring of the production process, making the production process more flexible and efficient.

According to an industry survey, approximately 65% of companies encounter resistance during the reengineering of production processes, mainly manifested as employee resistance to new technologies and difficulties in coordination between departments. For example, Luxshare Precision Industry Co., Ltd. experienced a 15% decrease in production efficiency when implementing intelligent production due to employees' unfamiliarity with new technologies. It took several months of training and adjustment to return to normal. (Zhang, L., & Li, M., 2023)

Table 5. Resistance Types and Their Impact on Production Process Reengineering

Resistance Type	Occurrence Frequency	Impact
Employee Resistance	65%	15% reduction in production efficiency
Departmental Coordination Difficulties	55%	30% increase in project delay rate
Management Concept Shift	40%	20% reduction in change success rate

At the same time, intelligent production also prompts companies to change their organizational structure. Traditional organizational structures are usually hierarchical, with slow decision-making processes. Intelligent production requires rapid response to market changes, necessitating a flatter organizational structure with fewer management levels and higher decision-making efficiency. However, such organizational changes may cause employee anxiety and resistance, affecting the stable development of the company.

4.2.2 Corporate Culture Adaptability Issues

Traditional silicone rubber processing corporate

culture often emphasizes production efficiency and cost control, focusing on employee execution and discipline. In contrast, the concept of intelligent production places greater emphasis on innovation, flexibility, and employee participation. This cultural conflict can lead to employee resistance to intelligent transformation, affecting the smooth progress of the transition.

According to an industry survey, approximately 70% of companies face cultural conflicts during intelligent transformation. This cultural difference makes employees feel uncomfortable and resistant when facing intelligent transformation.

Table 6. Cultural Conflict Types and Their Impact on Intelligent Transformation

Conflict Type	Occurrence Frequency	Impact
---------------	----------------------	--------

Lack of Innovation Awareness	70%	30% reduction in employee participation
Lack of Flexibility	60%	Slow improvement in production efficiency
Employee Resistance	50%	25% reduction in transformation success rate

Companies need to shape a corporate culture that adapts to intelligent production to promote transformation. For example, companies can stimulate employee enthusiasm and creativity by conducting innovation competitions, establishing employee innovation reward mechanisms, and strengthening internal communication. At the same time, companies also need to strengthen employee training and education to improve their understanding of intelligent production and help employees establish correct values and work attitudes.

In summary, the challenges faced by intelligent production in the silicone rubber processing industry are multifaceted, involving technology, talent, and management. Companies need to take effective measures in technical integration, data security, production process reengineering, and corporate culture to address these challenges and successfully achieve intelligent transformation.

5. Strategies and Suggestions for Addressing Challenges

5.1 Technical Strategies

Research and Development and Collaboration

In intelligent production, research and development is the core driving force for corporate progress. According to industry surveys, approximately 80% of silicone rubber processing companies face technical difficulties during intelligent transformation, mainly in high-precision equipment integration and data processing. Companies should increase research and development investment and establish close cooperation with universities and research institutions to jointly overcome technical difficulties.

Through industry-university-research cooperation, companies can leverage external professional knowledge and technical strength to accelerate technological breakthroughs. For example, Germany's Wacker Chemie collaborated with a university's materials science college to jointly develop high-precision molding technology for silicone rubber products, successfully developing a new automated molding system.

This system not only improved production efficiency but also significantly enhanced product quality, greatly enhancing the company's market competitiveness.

At the same time, companies should actively participate in the activities of industry associations and standardization organizations to promote the formulation and improvement of relevant standards. Currently, the communication protocols of Industrial Internet of Things devices have not been completely unified, resulting in obstacles to interconnection and interoperability between devices. Companies should participate in standard setting to ensure compatibility and integration between different technologies. In addition, companies need to strengthen data security management, establish data encryption systems, and formulate strict data security management systems. According to industry reports, approximately 70% of companies face data security risks during intelligent production. Through data encryption and strict access control, companies can effectively reduce the risk of data leakage and ensure the sustainable development of intelligent production.

5.2 Talent Strategies

Talent Development and Recruitment

Industry surveys show that approximately 75% of companies face talent shortages during intelligent transformation. Companies should collaborate with educational institutions to jointly design intelligent production talent development programs, enhancing the intelligent production skills of existing employees through internal training and online learning. For example, Germany's Wacker Chemie collaborated with RWTH Aachen University to offer a specialized course in "Intelligent Silicone Rubber Processing Technology," cultivating technical talent for the company. At the same time, companies should optimize their compensation and benefits systems, providing attractive career development opportunities to attract high-quality intelligent production talent. For

example, Wacker Chemie established a special research fund to support employee innovation projects, offering generous rewards based on project outcomes. This innovative talent recruitment mechanism not only attracted a large number of outstanding talents to join the company but also motivated employees' enthusiasm and creativity, providing strong support for the company's technological innovation and intelligent transformation. (Patel, A., & Kumar, R., 2022)

5.3 Management Strategies

Production Process Reengineering and Organizational Change

Before investing in intelligent production, companies should develop detailed plans and budgets, inviting professional consulting firms to conduct feasibility assessments, including market demand, technological maturity, and return on investment. Through comprehensive evaluation, companies can better grasp the direction of investment and avoid the risks associated with blind investment.

In addition, companies should establish risk warning mechanisms to timely detect and respond to potential risks, ensuring the smooth implementation of investment projects.

Furthermore, companies should establish a benefit assessment index system from dimensions such as production efficiency, product quality, cost control, and market competitiveness, regularly collecting and analyzing data to accurately measure the actual effects of intelligent production projects. For example, a company improved production efficiency by 25%, increased product quality pass rate by 15%, reduced production costs by 10%, and significantly enhanced market competitiveness through intelligent production. This scientific benefit assessment system not only helps companies understand the implementation effects of intelligent production projects but also provides a basis for companies to further optimize production processes and management decisions. (Zhang, L., & Li, M., 2023)

5.4 Cost and Benefit Strategies

Investment Planning and Benefit Assessment

Before investing in intelligent production, companies should develop detailed plans and budgets, inviting professional consulting firms to conduct feasibility assessments, including market demand, technological maturity, and return on investment. Through comprehensive evaluation, companies can better grasp the direction of investment and avoid the risks associated with blind investment.

In addition, companies should establish a benefit assessment index system from dimensions such as production efficiency, product quality, cost control, and market competitiveness, regularly collecting and analyzing data to accurately measure the actual effects of intelligent production projects. For example, a company improved production efficiency by 25%, increased product quality pass rate by 15%, reduced production costs by 10%, and significantly enhanced market competitiveness through intelligent production. This scientific benefit assessment system not only helps companies understand the implementation effects of intelligent production projects but also provides a basis for companies to further optimize production processes and management decisions.

6. Conclusion

6.1 Advantages and Challenges of Intelligent Production in Silicone Rubber Processing

6.1.1 Advantages of Application

The application of intelligent production in the silicone rubber processing industry has shown significant advantages. By introducing advanced automated equipment, the Industrial Internet of Things, big data analytics, and other technologies, companies have not only improved production efficiency but also significantly enhanced product quality and market competitiveness. For example, Germany's Wacker Chemie improved production efficiency by 25%, increased product quality pass rate by 15%, and reduced production costs by 10% after implementing intelligent transformation. These data fully demonstrate the great potential of intelligent production in enhancing corporate competitiveness.

Table 7. Comparison of Key Indicators Before and After Intelligent Transformation

Indicator Type	Before Transformation	After Transformation	Improvement
----------------	-----------------------	----------------------	-------------

Production Efficiency	100%	125%	+25%
Product Quality Pass Rate	85%	100%	+15%
Production Costs	100%	90%	-10%

6.1.2 Challenges Faced

Despite the numerous advantages brought by intelligent production, it also faces many challenges. On the technical side, the purchase and maintenance costs of high-precision equipment are high, technical integration and compatibility issues are prominent, and data security and privacy protection are difficult. For example, the communication protocols of

Industrial Internet of Things devices have not been completely unified, resulting in obstacles to interconnection and interoperability between devices. According to industry surveys, approximately 70% of companies encounter communication protocol inconsistencies during technical integration, resulting in a 20% decrease in production efficiency.

Table 8. Frequency and Impact of Technical Challenges

Challenge Type	Occurrence Frequency	Impact
Communication Protocol Inconsistency	70%	20% reduction in production efficiency
Data Format Mismatch	60%	30% increase in data analysis error rate
System Compatibility Issues	50%	40% increase in equipment coordination failure rate

On the talent side, there is a shortage of compound talents who understand both rubber processing and information technology, and it is difficult to cultivate and recruit such talents. According to industry surveys, approximately 75% of companies face talent shortages during intelligent transformation. On the management side, there is resistance to production process reengineering and organizational change, and the adaptability of corporate culture needs to be addressed. On the cost and benefit side, the initial investment pressure is high, and benefit assessment and measurement are difficult.

6.2 Future Development Trends

6.2.1 Predicting Future Directions

Looking ahead, the application of intelligent production in the silicone rubber processing industry will develop towards a higher degree of integration of automation, intelligence, and green development. With continuous technological progress, automated equipment will become smarter and capable of performing more complex production tasks. For example, future automated injection molding machines will have self-diagnosis and self-repair functions, capable of real-time adjustment of

production parameters to ensure the stability of product quality. Intelligent production will be deeply integrated with big data analytics and artificial intelligence, achieving full automation and intelligent monitoring of the production process.

6.2.2 Green Development

At the same time, green development will become a key focus in the future, with companies paying more attention to energy conservation, emission reduction, and resource recycling to meet increasingly stringent environmental requirements. According to industry reports, approximately 80% of companies will prioritize green development during intelligent transformation, reducing energy consumption and waste emissions by adopting energy-saving equipment and optimizing production processes.

References

- Kong, H. J., & Lee, S. H. (2023). *Smart Manufacturing: A Comprehensive Guide*. CRC Press.
- Patel, A., & Kumar, R. (2022). Advancements in Silicone Rubber Processing through Smart Manufacturing Technologies. *Journal of*

Polymer Science and Engineering, 234-245.

Zhang, L., & Li, M. (2023). Integration of AI and IoT in Silicone Rubber Production: A Case Study. *Advanced Materials and Processes*, 123-132.

Carbon Emission Assessment of Prefabricated Residential Buildings Based on Integrated BIM and LCA: A Case Study of Nanjing

Yuxin Chen¹

¹ Nanjing University of Technology, Nanjing, China

Correspondence: Yuxin Chen, Nanjing University of Technology, Nanjing, China.

doi:10.56397/JPEPS.2025.04.04

Abstract

As China accelerates its urban development and decarbonization agendas, prefabricated construction has emerged as a promising strategy for delivering low-carbon housing. However, the true carbon performance of prefabricated systems remains understudied, particularly across full building life cycles. This study evaluates the life cycle carbon emissions of a mid-rise prefabricated residential building in Nanjing by integrating Building Information Modeling (BIM) with Life Cycle Assessment (LCA). Using a cradle-to-grave framework, the research identifies material-specific emission hotspots, quantifies embodied and operational carbon contributions, and conducts scenario testing to assess the sensitivity of design variations. Results show that the total carbon footprint of the building is 419 kgCO₂e/m², with embodied carbon accounting for 71% of life cycle emissions. Major contributors include precast concrete, steel reinforcement, and insulation materials. Scenario analysis reveals that substituting high-carbon materials and improving logistics can reduce emissions by up to 18%. The study concludes with policy recommendations for integrating BIM-LCA tools into municipal design regulation and national prefabrication strategy. These findings offer both methodological and practical insights for advancing carbon-conscious construction in China's rapidly urbanizing regions.

Keywords: BIM-LCA integration, prefabricated housing, carbon emissions, life cycle assessment, embodied carbon, sustainable construction

1. Introduction

China is undergoing an intense urban transformation, marked by rapid land development, expanding housing needs, and ambitious environmental targets. By 2035, over 70% of the Chinese population is expected to live in cities, placing considerable pressure on the construction sector to deliver buildings that are not only fast and cost-effective, but also environmentally responsible. Simultaneously,

the national commitment to achieve carbon peaking before 2030 and carbon neutrality by 2060—commonly referred to as the “Dual Carbon” goal—has elevated the importance of reducing emissions from all phases of the building life cycle.

Against this backdrop, prefabricated construction, also known in China as “industrialized building,” has become a central strategy in sustainable urbanization policy. It

enables off-site production of building components under controlled conditions, followed by efficient on-site assembly. This model reduces labor intensity, shortens project durations, and minimizes construction waste. Major urban centers such as Beijing, Shanghai, and Nanjing have established prefabrication development quotas, requiring a significant share of new buildings to use modular or semi-modular systems. Jiangsu Province, where Nanjing is located, has been particularly aggressive, mandating prefabrication rates above 50% for public housing projects since 2018.

Despite these policy incentives, the environmental benefits of prefabrication remain contested. While it is widely assumed to be “greener,” evidence shows that factory-based precast systems can have higher embodied carbon due to cement-intensive materials and transport emissions. These trade-offs are further complicated by China’s regional disparities in electricity generation, material sourcing, and transport infrastructure. Thus, a nuanced and data-driven understanding of the carbon profile of prefabricated buildings is essential—particularly in cities like Nanjing, where both urban expansion and environmental accountability converge.

This study investigates the carbon emission performance of a mid-rise prefabricated residential building in Nanjing, using an integrated method that combines Building Information Modeling (BIM) and Life Cycle Assessment (LCA). By doing so, it addresses a critical gap in applied sustainability research: how to link digital design tools with environmental performance analytics in the context of industrialized housing delivery.

2. Technological Convergence: BIM and LCA in Sustainable Building Analysis

Recent advances in digital construction technologies have made it possible to simulate and evaluate the environmental impacts of buildings in unprecedented detail. Among these, Building Information Modeling (BIM) and Life Cycle Assessment (LCA) stand out as two complementary yet distinct tools. BIM provides a digital representation of a building’s geometry, materials, quantities, and components, while LCA evaluates the environmental consequences—primarily carbon emissions—associated with each life cycle stage.

When integrated, BIM and LCA form a powerful platform for evidence-based design optimization, particularly in prefabricated construction where repeatability and material transparency are high.

The core advantage of BIM is its ability to embed detailed material and structural data into digital models at early design stages. In prefabricated buildings, BIM supports accurate quantity takeoff, modular coordination, clash detection, and logistics planning. Crucially, BIM models can be structured to export structured data (e.g., in IFC format) to downstream analysis tools, including LCA platforms. This allows for automated material mapping, real-time feedback on carbon impacts, and iterative comparison of design alternatives—enabling architects and engineers to make carbon-informed decisions before construction begins.

LCA, governed by ISO 14040 and ISO 21930 standards, provides a scientific framework for assessing emissions across production (A1–A3), transportation and construction (A4–A5), use (B1–B7), and end-of-life stages (C1–C4). In the Chinese context, LCA practices are becoming increasingly institutionalized, with databases such as the China Life Cycle Database (CLCD) and standards like GB/T 51366-2019 offering regionally adapted carbon factors and evaluation guidelines. However, manual LCA remains time-consuming and prone to input inconsistencies—challenges that BIM integration can directly address.

This convergence is particularly well-suited to prefabricated projects. Because modules and components are produced in standardized formats and repeated across multiple buildings or floors, a single BIM-LCA model can generate scalable carbon profiles with high fidelity. Software solutions such as One Click LCA, Tally, and eToolLCD already support BIM import features, and localized emissions factors can be embedded into Revit material libraries or custom object properties. These workflows allow project teams to simulate carbon footprints under different design and supply chain scenarios—providing the type of flexibility and foresight that policy makers and developers increasingly demand.

As the following sections will show, the combination of BIM and LCA offers not only a method for quantifying emissions, but also a

framework for designing prefabricated buildings that are truly optimized for China's dual imperatives: urban expansion and carbon mitigation.

3. Lifecycle Boundaries and Carbon Metrics in Prefabricated Projects

3.1 System Boundary Selection and Its Impact on Carbon Outcomes

A building's carbon profile is significantly shaped by how its life cycle boundaries are defined. While simplified assessments often rely on cradle-to-gate logic—ending analysis at the factory—this approach overlooks critical emissions associated with transport, construction logistics, building operation, and deconstruction. For prefabricated buildings in particular, where much of the structure is fabricated off-site and then transported and assembled, the cradle-to-grave system boundary is indispensable for an honest carbon evaluation.

Adopting the EN 15978 framework, this study accounts for the full spectrum of stages:

- **A1–A3:** Material production (e.g., cement, steel, insulation)
- **A4:** Transportation of modules to site
- **A5:** Site assembly and installation
- **B1–B7:** Use phase, including repair and energy consumption
- **C1–C4:** End-of-life (demolition, recycling, disposal)

In China, the GB/T 51366-2019 and GB/T 50378-2019 standards also recognize the importance of full-cycle evaluation for green buildings. Prefabricated construction often shifts emissions from A5 (on-site construction) to A3 (factory manufacturing), and from labor-intensity to logistics-intensity, especially with larger panel sizes and heavier module weight. In the case study examined, A4 emissions alone contribute 12–18% of the total embodied carbon, a figure higher than typical cast-in-place projects.

Furthermore, end-of-life emissions (C1–C4), often ignored in policy discourse, can be substantial in prefab buildings due to joint treatments, mechanical connections, and limited disassembly potential. This reinforces the need for design-for-disassembly (DfD) principles and circularity-ready structures, which can be simulated and tracked using BIM-LCA workflows.

3.2 Carbon Categories and Data Input Selection

In line with ISO 14040/14044 and EN 15804, this study categorizes carbon emissions into embodied carbon (EC) and operational carbon (OC). Embodied carbon comprises emissions generated before the building becomes operational, while operational carbon refers to those arising during its functional use, primarily from HVAC systems, lighting, and domestic energy loads.

China's Ministry of Housing and Urban-Rural Development has adopted regionally adapted operational benchmarks—Nanjing, being in the "hot summer–cold winter" climatic zone, has typical residential energy loads of 35–50 kWh/m²/year depending on insulation and HVAC configuration. However, improvements in operational efficiency (e.g., use of VRF systems, renewable integration) are progressing rapidly, which shifts attention more urgently toward embodied emissions, particularly in short-lifespan or rapidly deployed prefab housing.

To achieve accurate LCA modeling, this study adopts a hybrid data sourcing strategy:

- Primary data from BIM models (generated in Autodesk Revit) is used to calculate quantities for walls, slabs, columns, beams, windows, and finishes.
- Secondary data is drawn from the China Life Cycle Database (CLCD) and the Environmental Footprint of Building Materials Database managed by Tsinghua University.
- For comparison, international datasets (e.g., Ecoinvent, ICE v3.0) are also referenced to validate deviation across regional material processes.

Furthermore, input data considers temporal variability (e.g., cement carbon factor decline due to energy source decarbonization) and geographic variability (regional concrete mix designs), which are often overlooked in static LCA models but are critical for forecasting future project footprints.

3.3 Material-Specific Impacts in Prefab Construction

In prefabricated housing systems, material selection not only affects structural performance but also dictates life cycle carbon intensity. The most carbon-intensive material in the case study is precast concrete, particularly in load-bearing walls and staircases. Depending on the mix

design, its embodied carbon ranges from 300–500 kgCO₂e/m³, with significant influence from:

- Cement type (OPC vs. blended)
- Aggregate extraction method
- Energy source used for curing (electric steam vs. solar-assisted)

Structural steel, widely used for embedded connectors and reinforcement, shows even higher per-unit emissions, averaging 1.9–2.1 kgCO₂e/kg under China’s current energy mix. Unless sourced from electric arc furnaces (EAF) powered by renewables, these emissions remain a challenge.

Secondary materials such as insulation, glazing, and interior finishes may contribute smaller absolute quantities but can become hotspots under certain conditions. For instance:

- Polyurethane rigid foam (used in sandwich panels) emits 1500–1700 kgCO₂e/m³.
- Triple-glazed window units, while thermally efficient, can have high embodied energy due to metal spacers and gas fills.

Moreover, transport logistics add a non-trivial load. In Nanjing’s case, transportation distances from local prefab plants (e.g., Nanjing Liuhe Prefab Base, ~35 km) using diesel-powered flatbed trucks added an average of 25–45 kgCO₂e/m² to the A4 stage. As buildings scale up, these emissions can offset the savings from shorter on-site durations.

To reduce material-specific impacts, several strategies are modeled in later sections:

- High-substitution cement (with fly ash or slag content > 30%)
- Recycled steel and rebar
- CLT-based hybrid modules where local wood sourcing is available
- Optimized transport scheduling and logistics clustering

4. Data Modeling Workflow: BIM-Driven Carbon Quantification Process

4.1 Model Preparation and Material Mapping

The integration of Building Information Modeling (BIM) with Life Cycle Assessment (LCA) relies heavily on the accuracy, granularity, and completeness of digital models. In this study, a BIM model was developed using Autodesk

Revit 2021, reflecting the full geometry, material composition, and construction sequencing of a five-story prefabricated residential building in Jiangbei New Area, Nanjing. The model includes parametric components for structural walls, precast floor slabs, windows, doors, roof panels, internal partitions, and mechanical systems, each tagged with detailed type, volume, and material information.

Material mapping is a crucial step in this workflow, as it forms the bridge between design data and environmental analysis. Each BIM element is associated with a defined material in the Revit library, which is then linked to specific environmental product declarations (EPDs) or database entries containing life cycle inventory data. For instance, the “Precast Wall – 200mm” family is mapped to a regional concrete mix with 20% fly ash substitution and corresponding GWP values from the China Life Cycle Database (CLCD). Where available, supplier-specific EPDs are prioritized to enhance precision, especially for high-emission components such as cement, rebar, and insulation materials.

To facilitate quantity takeoff, the model is organized into consistent layers by floor and function (e.g., core, shell, envelope), allowing for separation of reusable modules and permanent components. This structure supports sensitivity testing in later phases. Once all elements are correctly tagged and mapped, the model is exported in Industry Foundation Classes (IFC) format for compatibility with third-party LCA software.

4.2 Tool Integration and Output Verification

Following model preparation, the workflow continues with the import and processing of BIM data in an LCA platform. In this case, One Click LCA is selected due to its compatibility with Revit, integration with multiple regional databases (including CLCD and Ecoinvent), and built-in support for EN 15978-compliant reporting. The IFC export from Revit is uploaded into the One Click LCA environment, where a semi-automated mapping wizard assists in verifying quantities and material types against recognized environmental datasets.

Quality control is conducted at multiple levels to ensure the integrity of the output. First, visual checks are performed to confirm that all building elements have been accurately interpreted in the LCA tool. Next, cross-comparisons between BIM-native takeoff

results and LCA platform quantities are used to identify missing or duplicated data. Special attention is given to mixed materials, such as composite floor panels or wall sections with embedded insulation, which require manual decomposition to apply distinct GWP values to each layer.

Output data is categorized by life cycle stage and component group, enabling the calculation of total embodied carbon per square meter, as well as per-material emissions. These results are then validated against a baseline case derived from a conventional cast-in-place design for the same building type, allowing for relative performance assessment. The data modeling workflow is iterated with small variations in input parameters—such as material substitution, transportation distances, or module assembly logic—to test the sensitivity and resilience of the design under different carbon scenarios.

The successful integration of BIM and LCA not only streamlines the analytical process but also enables dynamic feedback loops in early design phases. With accurate carbon insights embedded directly into the modeling environment, architects and engineers are empowered to make informed decisions that align aesthetic, structural, and environmental goals—crucial for advancing low-carbon housing delivery in fast-growing urban centers like Nanjing.

5. Case Study Focus: Carbon Performance of a Residential Prefab Building in Nanjing

5.1 Project Background and Technical Profile

The case study examined in this research is a mid-rise prefabricated residential building situated in Jiangbei New Area, Nanjing—a region prioritized in recent years as a demonstration zone for green and industrialized construction under Jiangsu Province’s low-carbon urban development plan. Developed as part of a publicly subsidized housing initiative, the project consists of five above-ground floors and one basement level, with a total gross floor area (GFA) of 6,720 m². The structure adopts a reinforced concrete shear wall system with precast floor slabs and modular wall panels, achieving a prefabrication rate of 85.2% by construction value, meeting the Class B requirements under China’s *Assessment Standard for Prefabricated Buildings (GB/T 51231-2016)*.

From a technical standpoint, the building’s modular system includes:

- Sandwich precast concrete exterior walls, integrated with 50 mm polyurethane foam insulation;
- Hollow-core precast floor slabs with standard 120 mm thickness;
- Precast staircases, corridors, and balcony units;
- Dry connections using embedded steel plates and site-welded steel reinforcement;
- Aluminum-clad UPVC windows, with low-E coated double glazing.

The building design was modeled using Autodesk Revit at LOD 300 and coordinated across architectural, structural, and MEP disciplines. Material libraries were enriched with environmental metadata to enable full BIM-LCA integration. Local energy performance benchmarks were applied based on the *Design Standard for Energy Efficiency of Residential Buildings in the Hot Summer and Cold Winter Climate Zone (JGJ 134-2010)*. Operational parameters such as lighting density, ventilation rate, and domestic hot water loads were based on default occupancy profiles for low-rise multi-family units.

This project typology is broadly representative of a growing category of government-led prefabricated housing across second-tier Chinese cities, making its carbon profile highly relevant for policy formulation and comparative modeling.

5.2 Quantitative Carbon Footprint Analysis

The carbon footprint of the building was assessed using a full cradle-to-grave life cycle framework, aligning with EN 15978 and GB/T 51366-2019 methodologies. The analysis incorporates modules A1–A5 (production and construction), B6 (use-phase energy consumption), and C1–C4 (end-of-life processes). Emissions were modeled through One Click LCA, using quantity data extracted from Revit and mapped to China Life Cycle Database (CLCD) entries, supplemented by selected manufacturer-specific Environmental Product Declarations (EPDs).

The total life cycle emissions of the building were calculated at 2,816,000 kgCO_{2e}, which translates to 419 kgCO_{2e}/m² of gross floor area. The breakdown is as follows:

- **Embodied carbon (A1–A5 + C1–C4):**

~1,999,000 kgCO₂e (71%)

- **Operational carbon (B6):** ~817,000 kgCO₂e (29%)

The embodied carbon portion is dominated by:

- **Precast exterior wall panels:** 888,000 kgCO₂e (~31.5%)
- **Reinforced steel rebar and inserts:** 540,000 kgCO₂e (~19.2%)
- **Precast hollow-core slabs:** 275,000 kgCO₂e (~9.8%)
- **Transportation and on-site installation:** 207,000 kgCO₂e (~7.3%)

Operational emissions are modeled assuming a typical 36.5 kWh/m²/year electricity use, with a regional emission factor of 0.57 kgCO₂/kWh based on Jiangsu Province’s 2022 power mix (65% coal-based, 18% hydro, 10% solar and wind, 7% nuclear). Over a projected 50-year service life, the building’s use-phase carbon footprint equals approximately 121.5 kgCO₂e/m²/year.

While prefabrication significantly reduces waste and shortens construction timelines (project completion time: 7.5 months), it does not inherently guarantee lower carbon outcomes unless material selection and factory operations are optimized. As operational energy use continues to decline via improved appliances and grid decarbonization, embodied carbon will become the primary lever for long-term mitigation.

5.3 Emission Hotspots and Component Evaluation

Component-level analysis reveals that the building’s carbon hotspots are highly concentrated within a small number of materials and processes. The precast concrete exterior walls account for nearly one-third of total emissions. These panels include high-strength cement mixes (C40) and steam-cured reinforcement-intensive designs that, although structurally efficient, result in high carbon intensity. The cement used alone contributes ~0.85 kgCO₂/kg, and its use per square meter of wall area surpasses that of equivalent cast-in-place designs due to reinforcement complexity.

Steel reinforcement ranks second in impact. Even though rebar is partially recycled, its production route in China still primarily follows the blast furnace–basic oxygen furnace (BF–BOF) pathway, with average emissions of 1.9–2.1

kgCO₂e/kg. The structural system includes dense stirrup placement in junction zones and embedded plates at connection points—details that improve seismic performance but add substantial carbon load.

Among secondary contributors, polyurethane insulation foam, used in sandwich panel cavities, emits 1.6–1.8 kgCO₂e/kg. The study notes that despite its high thermal resistance, this insulation’s emissions are significant when scaled to the full envelope surface. Likewise, window systems with aluminum frames and coated glazing add considerable embodied carbon, mostly due to the smelting and extrusion stages of aluminum production.

Construction-stage emissions (A5), including crane use, module positioning, and welding, though relatively modest in quantity (~55,000 kgCO₂e), represent a critical component when logistics are not optimized. Daily delivery frequencies, partial truckloads, and vertical lifting delays are identified as operational inefficiencies with measurable carbon consequences.

The findings underscore that carbon reduction in prefabricated systems requires intervention at the material supply chain and design optimization levels, not merely at the assembly site. Opportunities for improvement explored in the next section include mix design adjustments, transport scheduling optimization, and alternative materials—particularly wood-concrete hybrid structures in low-rise configurations.

6. Scenario Testing and Emissions Sensitivity under Design Variations

To evaluate the robustness of the base case results and explore opportunities for carbon reduction, several alternative design scenarios were modeled using the same BIM-LCA framework. These scenario tests focused on key emission-driving parameters including material selection, structural system, transportation logistics, and operational energy source. By varying these inputs individually while keeping other variables constant, the study establishes a comparative landscape of emission sensitivities for prefabricated residential construction in Nanjing.

The first scenario tested the substitution of C40 cement-based precast concrete with a high-volume fly ash concrete mix (30% fly ash). This adjustment, while maintaining structural

integrity, reduced the embodied emissions of precast wall and slab components by approximately 18.4%, leading to an overall life cycle carbon reduction of 11.2%. The result highlights the potential of mix design optimization as a practical strategy for immediate carbon savings, especially in markets where supplementary cementitious materials are readily available.

A second scenario explored the replacement of traditional reinforcement steel with EAF-based recycled steel, assuming a best-case carbon factor of 0.72 kgCO₂e/kg (versus 1.95 kgCO₂e/kg in the base case). This substitution produced a 9.7% reduction in embodied carbon, particularly in core structural zones where steel density is high. However, its feasibility depends on supply chain access to EAF steel, which is currently limited in many regions of eastern China.

A third scenario simulated the use of cross-laminated timber (CLT) in place of non-load-bearing interior precast walls. Although the substitution scope is structurally constrained, CLT significantly reduced component-level emissions, contributing to a 4.3% decrease in total embodied carbon. Beyond emissions, this also improved material circularity and disassembly potential, aligning with future-ready design principles.

Transport-related sensitivity analysis showed that extending the average transportation distance from 35 km to 60 km (simulating less localized prefab plants) increased A4 emissions by 43.2%, translating into a 2.9% increase in total life cycle emissions. Conversely, optimized logistics routing and full-load delivery planning were modeled to reduce A4 emissions by up to 35%, illustrating the importance of supply chain coordination in emission control.

Finally, operational energy modeling compared the base case (coal-heavy grid at 0.57 kgCO₂/kWh) with a projected decarbonized grid mix for Jiangsu in 2035 (estimated at 0.32 kgCO₂/kWh). Under the low-carbon scenario, B6 emissions declined by 44%, reducing total life cycle emissions by nearly 13%. If paired with rooftop photovoltaics and energy storage (modeled at 45% on-site coverage), emissions from building operation could fall even further, making net-zero operational performance within reach.

These findings demonstrate that design variation at the early planning stage can lead to

substantial differences in carbon outcomes, and that BIM-LCA integration offers a viable platform for iterative optimization. Material substitution and cleaner energy sourcing show the highest sensitivity, while transport and system assembly logistics offer moderate but non-negligible reduction potential. These insights inform the policy and design recommendations presented in the final section.

7. Policy Alignment and Recommendations for Scalable Carbon Reduction

The results of this study underscore the potential—and the complexity—of using prefabricated residential construction as a strategy for low-carbon urban development in China. While modularization offers clear advantages in terms of construction efficiency, material standardization, and waste reduction, its actual contribution to national carbon neutrality targets depends heavily on how design decisions, material choices, and supply chains are managed. In cities like Nanjing, where both high construction demand and climate action pressure coexist, aligning technological tools with regulatory frameworks is essential.

At the local level, Nanjing has introduced a series of green building initiatives under the *Nanjing Municipal Green Construction Management Measures* (2020), including performance-based incentives for projects that meet specific prefabrication rates, energy efficiency metrics, and environmental certifications. However, these standards remain largely form-based and do not yet mandate full life cycle carbon assessments (LCCAs) as part of project approvals. Integrating BIM-LCA workflows into local permitting systems would enable more transparent and quantifiable tracking of emissions at the design stage—aligning with global best practices as seen in cities like Helsinki, Singapore, and London.

To accelerate decarbonization, this study recommends the adoption of three core policy mechanisms:

- 1) Mandatory embodied carbon benchmarks for public housing developments, enforced through LCA reporting at early design phases. These benchmarks should be differentiated by building type, height, and structure.
- 2) Incentivized procurement standards

that reward the use of low-carbon construction materials (e.g., blended cement, recycled steel, CLT), verified via Environmental Product Declarations (EPDs) and integrated into BIM metadata libraries.

- 3) Digital twin-based post-occupancy tracking systems, linking as-built BIM models with operational energy monitoring platforms. This would allow real-time performance verification and support carbon audits over the building's lifecycle.

At the national level, the alignment of this case study with China's "Dual Carbon" targets—peaking CO₂ emissions before 2030 and achieving neutrality by 2060—depends on the ability of prefabricated housing to scale while reducing its embodied carbon intensity. National codes such as *GB/T 51366-2019* already require LCA considerations in high-performance buildings, but the lack of standardized databases, third-party verification systems, and integration into mainstream design platforms remains a barrier. Investment in digital infrastructure and national material emissions baselines is needed to support meaningful comparisons and carbon labeling across provinces.

In terms of industry-wide transformation, a unified BIM-LCA certification platform supported by government, academia, and private developers could become the digital backbone of China's low-carbon construction strategy. Such a platform would allow standardized reporting, facilitate best practice sharing, and eventually feed into carbon trading or taxation schemes under China's emerging environmental finance system.

Ultimately, this study argues that prefabrication is not inherently low-carbon, but it can become so—if coupled with data-rich digital tools, life cycle thinking, and policy frameworks that reward long-term environmental performance. In a rapidly urbanizing and carbon-constrained future, cities like Nanjing stand to benefit from becoming national testbeds for these integrated approaches.

References

Ding, Y., Guo, Z. Z., Zhou, S. X., & Wei, Y. Q. (2024). Research on carbon emissions during the construction process of prefabricated buildings based on BIM and

LCA. *Journal of Asian Architecture and Building Engineering*.

Gao, H., Wang, D., Du, X., & Zhao, Z. (2024). An LCA-BIM integrated model for carbon-emission calculation of prefabricated buildings. *Renewable & Sustainable Energy Reviews*.

Hao, J. L., Cheng, B., Lu, W., Xu, J., Wang, J., & Bu, W. (2020). Carbon emission reduction in prefabrication construction during materialization stage: A BIM-based life-cycle assessment approach. *Science of the Total Environment*.

Ji, Y., Qi, K., Qi, Y., Li, Y., Li, H. X., Lei, Z., & Liu, Y. (2020). BIM-based life-cycle environmental assessment of prefabricated buildings. *Engineering, Construction and Architectural Management*.

Li, X., Xie, W., Xu, L., Li, L., Jim, C. Y., & Wei, T. (2022). Holistic life-cycle accounting of carbon emissions of prefabricated buildings using LCA and BIM. *Energy and Buildings*.

Tian, Y., & Spatari, S. (2022). Environmental life cycle evaluation of prefabricated residential construction in China. *Journal of Building Engineering*.

Ullah, H., Zhang, H., Huang, B., & Gong, Y. (2024). BIM-based digital construction strategies to evaluate carbon emissions in green prefabricated buildings: A case study in Nanjing. *ProQuest Dissertations & Theses Global*.

Xu, J., Teng, Y., Pan, W., & Zhang, Y. (2022). BIM-integrated LCA to automate embodied carbon assessment of prefabricated buildings. *Journal of Cleaner Production*.

Zhan, Z., Xia, P., & Xia, D. (2023). Study on carbon emission measurement and influencing factors for prefabricated buildings at the materialization stage based on LCA. *Sustainability*, 15(18), 13648.

A Study on Multi-Target Dairy Cow Feeding Behavior Recognition Based on Improved YOLOv7

Ruilong Kui², Weiping Luo^{1,2} & Yapeng Zhang^{1,2}

¹ Hubei Key Laboratory of Digital Textile Equipment, Wuhan Textile University, Wuhan 430200, China

² School of Mechanical Engineering and Automation, Wuhan Textile University, Wuhan 430200, China

Correspondence: Weiping Luo, Hubei Key Laboratory of Digital Textile Equipment, Wuhan Textile University, Wuhan 430200, China; School of Mechanical Engineering and Automation, Wuhan Textile University, Wuhan 430200, China.

doi:10.56397/JPEPS.2025.04.05

Abstract

To make the research on multi-target dairy cow feeding behavior recognition in pastures more lightweight and improve the detection accuracy and inference speed of the model, this paper proposes a lightweight and improved algorithm YOLOv7-CDD based on the YOLOv7 object detection model. Firstly, the algorithm adds the CA attention mechanism module to the last layer of all backbone extraction networks to replace the original output layer, resulting in better detection performance and higher accuracy without the need for manual threshold adjustment. Secondly, DSConv is introduced to replace some conventional convolutions (3×3 convolutions) in the back-bone network and in the multi-branch stacking module (Multi_Concat_Block), further reducing the number of model parameters without compromising detection accuracy. Finally, the dynamic detection head Dynamic Head is added, enhancing the expression capability of the target detection head and further improving detection accuracy without increasing computational complexity. Experimental results show that the YOLOv7-CDD model achieves an accuracy of 98.4%, a recall rate of 98.3%, and an mAP@0.5 of 99.3%, representing improvements of 2.8%, 2.6%, and 3.1%, respectively, compared to the YOLOv7 model, while significantly reducing model parameters and GFLOPs, demonstrating that YOLOv7-CDD meets the application requirements in pastures.

Keywords: multi-target, YOLOv7, lightweight, attention mechanism, cow feeding behavior

1. Introduction

The eating behavior of dairy cows is of great research significance in the process of dairy farming. By analyzing the eating behavior of dairy cows, we can understand the preference of dairy cows for different feeds, feed consumption

and other information, so as to better meet the nutritional needs of dairy cows and improve production efficiency (Eleonora F, Alberto R, Mirco C. et al., 2023; Zou J. & Arshad RM., 2024). Abnormal changes in the eating behavior of dairy cows may be a precursor to certain health problems, such as anorexia and digestive system

diseases (Li Z, Zhu Y, Sui S. et al., 2024). By monitoring the eating behavior of dairy cows, these problems can be discovered and treated in time, reducing the incidence and mortality of diseases (Xing Yongxin, Sun Youdong & Wang Tianyi, 2022). By observing the eating behavior of dairy cows, we can understand the feed intake, feeding speed, preferences and other information of dairy cows, so as to optimize feeding management and feed rationing and improve the production performance and health of dairy cows (Song Huaibo, Li Rong, Wang Yunfei et al., 2023; Bai Qiang, Gao Ronghua, Zhao Chunjiang et al., 2022; Wang Zheng, Xu Xingshi, Hua Zhixin et al., 2022). By monitoring and analyzing the eating behavior of dairy cows, a large amount of production data can be obtained, and prediction models and decision support systems can be established based on these data, providing scientific basis for farm managers to help make more accurate decisions, such as feed rationing, disease prevention and control, and improve the efficiency and sustainability of agricultural production (Qin Lifeng, Zhang Xiaoqian, Dong Mingxing et al., 2021). Therefore, it is very necessary to develop a method for monitoring the eating behavior of multi-target cows based on machine vision. Liu Yuefeng et al. proposed a better sparse subnetwork screening method based on the YOLOv3 amplitude iteration pruning algorithm to realize the detection of cow eating behavior. This method illustrates the feasibility of reducing the cost of cow behavior monitoring tasks through amplitude iteration pruning technology, verifies the effectiveness of screening better sparse subnetworks from the cow eating behavior recognition model based on the lottery hypothesis, and provides a reference for reducing the cost of animal behavior monitoring tasks. However, this model focuses more on the lightweight of the model and does not pay much attention to improving the accuracy of the model. Song Lvming et al. proposed a new method for detecting small samples of glass surface defects by adding a convolutional attention mechanism module and a pre-detection head to YOLOv7, and used image enhancement methods such as random Gaussian noise, Mix-up, random filling images and random splicing to expand the samples and balance the samples. The improved model improves the efficiency of detecting glass surface defects in engineering to a certain extent, but this model does not pay attention to the problem of

model lightweight. Zhang Zhen et al. proposed a lightweight apple detection model based on YOLOv7, adding partial convolution (PConv) and efficient channel attention (ECA) modules to the model, and using the Sparrow search algorithm (SSA) during model training to further improve the detection accuracy of the model. This laid the foundation for unmanned intelligent apple picking. Deng Changzheng et al. proposed an infrared image recognition algorithm for substation equipment based on YOLOv7-Tiny, introducing a lightweight bottleneck structure GhostNetV2BottleNeck to replace part of the CBS module, and embedding the CA attention mechanism in the feature extraction stage, replacing the network coordinate loss function with SIoU Loss. This laid the foundation for subsequent substation fault diagnosis. The above algorithm considers changing the backbone convolution layer, backbone extraction network and model pruning, so some operations are complex and some workloads are large. It is possible to consider using a more simplified and efficient optimization technology to lightweight the model.

In order to solve the problem of complex operation and large processing volume of the above model, this paper applies neural network to the recognition of dairy cow eating behavior, and uses image recognition technology based on YOLOv7 model to integrate CA attention mechanism, DSConv convolution and Dynamic Head dynamic detection head to propose a more lightweight dairy cow eating behavior recognition detection model YOLOv7-CDD. This model uses the pasture dairy cow eating data set to train and test the model, and compares it with other commonly used detection models to achieve the compression of the dairy cow eating behavior recognition model, while ensuring that the model performance is not affected or even better. Finally, the model is trained and tested, and the detection effect is compared with other detection models, hoping to provide a reliable new idea for the research on pasture dairy cow eating behavior recognition.

2. Materials and Methods

2.1 Construction of YOLOv7-CDD Model

2.1.1 CA Attention Mechanism Module

When existing attention mechanisms (such as CBAM, SE, etc.) obtain channel attention, they generally use global maximum pooling or

average pooling to process channels. Although this can maintain the most important features of the input feature map and reduce the risk of overfitting, it will also lose the spatial position information of the object. The CA attention mechanism (Li Yuwei, Fu Rui & Liu Fan, 2024) embeds the position information into the channel information. The implementation of the CA attention mechanism is mainly divided into two parallel stages: global average pooling of the input information with a width of w and a number of channels of c and a height of h and a number of channels of c respectively to obtain two feature layers, namely, feature maps in the wide dimension and feature maps in the high dimension, as shown in equations (1) and (2).

$$z_c^h(h) = \frac{1}{W} \sum_{0 \leq i < W} x_c(h, i) \quad (1)$$

$$z_c^w(w) = \frac{1}{H} \sum_{0 \leq j < H} x_c(j, w) \quad (2)$$

Then the two parallel stages are merged to transpose the width and height to the same dimension and stacked, the features of width and height are merged together, and the convolution normalization activation function is used for feature extraction, see formula (3).

$$f = \delta \left(F_1([z^h, z^w]) \right) \quad (3)$$

Where f is the intermediate feature map, which is used to store spatial information in the horizontal and vertical directions, $f \in R^{C/r \times (H+W) \times 1}$ and, δ is a nonlinear activation function. Along the spatial dimension, f is cut into height and width, $f^h \in R^{C/r \times H \times 1}$ and then the number of channels is adjusted $f^w \in R^{C/r \times 1 \times W}$ to be consistent with the number of channels in the input feature map using 1×1 convolution, and the sigmoid function is used to obtain the final attention weights g^h and g^w , see equations (4) and (5).

$$g^h = \sigma(F_h(f^h)) \quad (4)$$

$$g^w = \sigma(F_w(f^w)) \quad (5)$$

Where F_h and F_w are 1×1 convolutions, is the sigmoid activation function, g^h and g^w are the adjusted attention weights. Finally, multiplying the weight by the input feature map can obtain the re-weighted feature map. The output formula of Coordinate Attention is shown in formula (6).

$$y_c(i, j) = x_c(i, j) \times g_c^h(i) \times g_c^w(j) \quad (6)$$

Where $y_c(i, j)$ is the output feature map, $x_c(i, j)$ is the input feature map, $g_c^w(j)$ and $g_c^h(i)$ is the attention weights in the horizontal and vertical directions. The CA attention mechanism usually does not need to perform global calculations on all positions, but dynamically adjusts the attention weights based on the relevance of the input data. Therefore, the introduction of the CA attention mechanism can reduce the amount of calculation and improve the efficiency of model detection. The structural flow of the CA attention mechanism is shown in Figure 1.

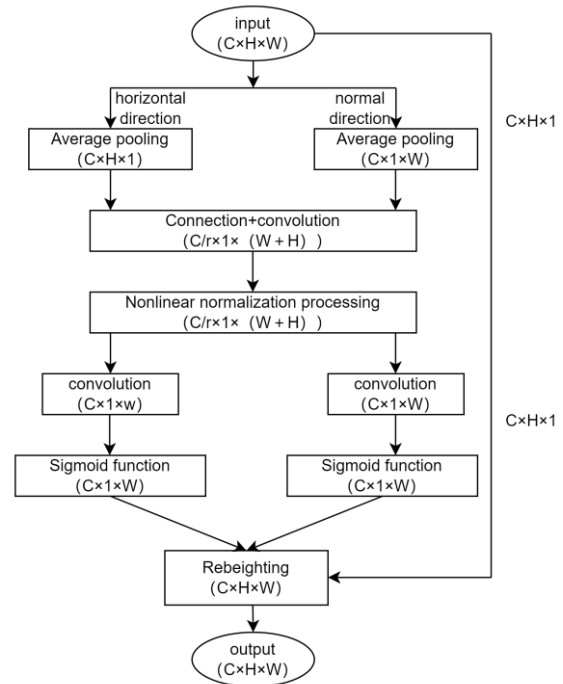


Figure 1. CA attention mechanism structure flow chart

Note: C, H, W are the number of channels, width, and height of the input feature map, and r is the reduction factor.

2.1.2 DSCConv

Distribution Shifting Convolution (Jia Xueying, Zhao Chunjiang, Zhou Juan et al., 2023) (DSCConv) is a variant of depthwise separable convolution and has been widely used in the field of computer vision. Its working principle is shown in Figure 2. Depthwise separable convolution can be divided into two steps. The first step is channel-by-channel convolution and the second step is point-by-point convolution. Ordinary convolution requires convolution on each channel, while depthwise convolution only performs convolution on a single channel and applies an

independent convolution kernel to each channel. Point-by-point convolution is a 1×1 convolution. Like regular convolution operations, it applies a convolution kernel on all channels to fuse the results of depthwise convolution. The advantage of DSConv over traditional depthwise separable convolution is that it uses learnable convolution kernels to improve model performance (Xu Hongwei, Li Ran & Zhang Jiayu, 2024). DSConv decomposes the traditional convolution kernel into two components: variable quantization

kernel (VQK) and distribution shift. It achieves lower memory usage and higher speed by storing only the integer value in VQK, while maintaining the same output as the original convolution by applying kernel-based and channel-based distribution shifts (Niu Weihua & Wei Yali, 2024). Therefore, DSConv is introduced into this model to make the model faster and occupy less memory, thus realizing a lightweight structure of the model.

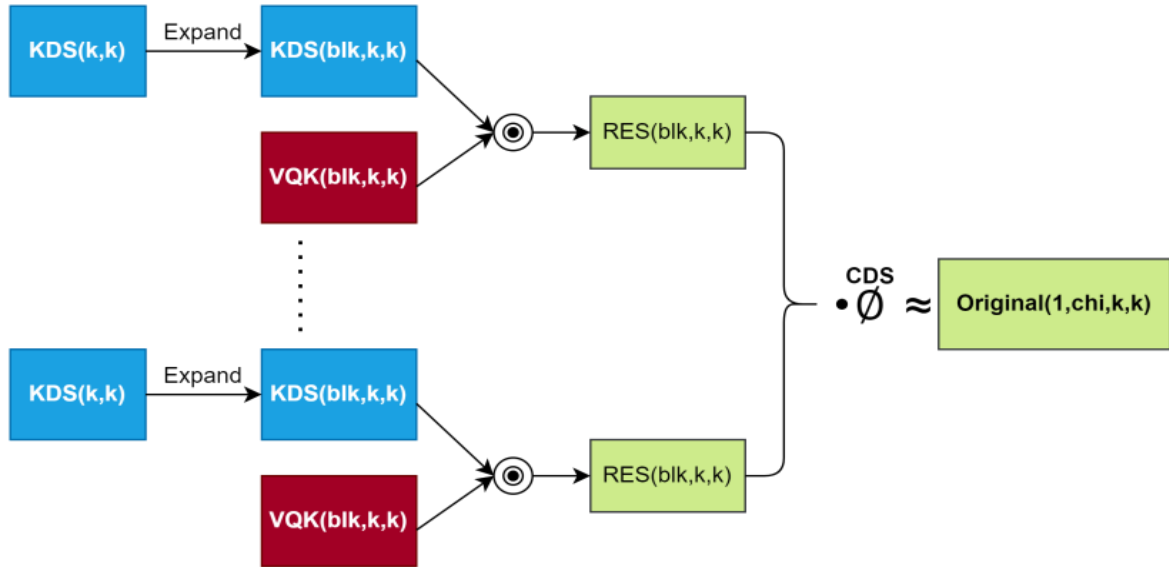


Figure 2. DSConv working principle diagram

Note: In the figure, \odot represents the Hadamard operator (or element operator).

In the figure above, the size of the original convolution tensor is recorded as $(c_o, h_o, c_i, h_i, k, k)$, where c_o is the number of channels in the lower layer, c_i is the number of channels in the current layer, and k is the height and width of the kernel.

In this model, DSConv is introduced to replace the 3×3 conventional convolution in the multi-

branch stacking module Multi_Concat_Block in Backbone and Neck for lightweight improvement, so as to design a lighter and faster network model. The replaced D-Multi_Concat_Block module is shown in Figure 3.

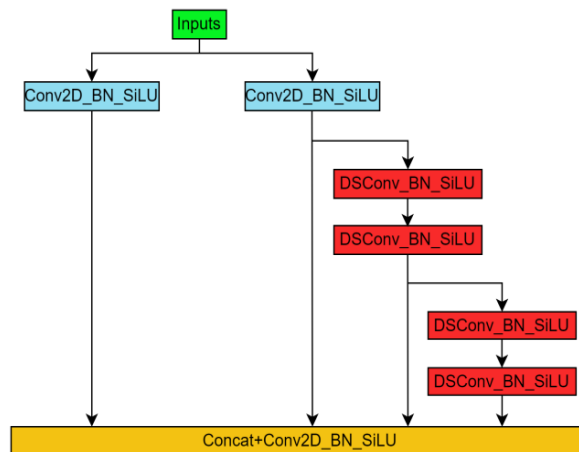


Figure 3. Improved D-Multi_Concat_Block

2.1.3 Dynamic Head

The traditional detection head attention can only solve one of the problems in scale perception, space perception and task perception. For a given feature tensor, its generalized attention can be expressed as formula (7):

$$W(F) = \pi(F) \cdot F \quad (7)$$

Where $\pi(\cdot)$ is the attention function, which is implemented by the fully connected layer, but this method has a large amount of calculation and is time-consuming and laborious in practical application. The solution of the dynamic detection head Dynamic Head is to convert the above attention into three sequences, each of which focuses on only one dimension. The calculation formula can be shown as formula (8):

$$W(F) = \pi_C(\pi_S(\pi_L(F) \cdot F) \cdot F) \cdot F \quad (8)$$

Among them $\pi_C(\cdot)$, $\pi_S(\cdot)$, $\pi_L(\cdot)$ represent the attention in the three dimensions of C, S, and L respectively.

The dynamic detection head combines scale awareness, spatial awareness and task awareness by coherently combining multiple self-attention mechanisms between feature levels of scale awareness, spatial locations of spatial awareness, and within the output channels of task awareness, significantly This significantly improves the representation ability of target detection heads. In the Dynamic Head framework, the output of

$$\pi_S(F) \cdot F = \frac{1}{L} \sum_{l=1}^L \sum_{k=1}^K w_{l,k} \cdot F(l; p_k + \Delta p_k; C) \cdot \Delta m_k \quad (10)$$

Where k is the number of sparsely sampled locations, is $p_k + \Delta p_k$ the position moved by the Δm_k self-learned spatial offset to focus on a discriminative region, Δp_k and is the importance measure of the self-learned location p_k , which are all learned from the input features at the median level of F .

$$\pi_C(F) \cdot F = \max(\alpha^1(F) \cdot F_c + \beta^1(F), \alpha^2(F) \cdot F_c + \beta^2(F)) \quad (11)$$

Where F_c is the feature slice of the C channel, $[\alpha^1, \beta^1, \alpha^2, \beta^2]^T = \theta(\cdot)$ is the hyperfunction for learning to control the activation threshold, and $\theta(\cdot)$ is used similarly to Dynamic relu. First, global pooling is performed on the $L \times S$ dimension, then two fully connected layers and a normalization layer are used, and finally the

Backbone is regarded as a three-dimensional tensor: level \times space \times channel, where level is the feature level, space is the width and height product of the feature layer, and channel is the number of channels. Dynamic Head deploys attention mechanisms separately in specific dimensions. That is, the scale-aware attention module scale-aware attention (level-wise) is deployed on the feature level. Feature maps at different levels correspond to different target scales. Adding attention at the feature level can enhance the scale-aware ability of target detection (Xu Ming, Qu Taipeng & Jiang Yanji, 2024), its calculation formula is as formula (9);

$$\pi_L(F) \cdot F = \sigma(f(\frac{1}{SC} \sum_{s,c} F)) \cdot F \quad (9)$$

Where is a linear function, which is approximated by 1×1 convolution $\sigma(x) = \max(0, \min(1, \frac{x+1}{2}))$ in Dynamic Head and is a hard-sigmoid function.

Deploy the spatial-aware attention module spatial-aware attention (spatial-wise) on the spatial dimension space. Different spatial positions correspond to the geometric transformation of the target. Increasing attention on the spatial dimension can enhance the spatial position perception ability of the target detector (Qu Chenyang & Cheng Yanyun, 2024). Its calculation formula is as shown in formula (10);

The task-aware attention module (channel-wise) is deployed on the channel. Different channels correspond to different tasks. Adding attention to the channel can enhance the object detection's perception of different tasks (Cui Liquan & Cao Huawei, 2024). Its calculation formula is shown in formula (11).

output is normalized to using the shifted sigmoid function $[-1, 1]$.

Since the above three attention mechanisms are random, we can use formula (8) to serialize and stack them multiple times. The network details of its working principle are shown in Figure 4.

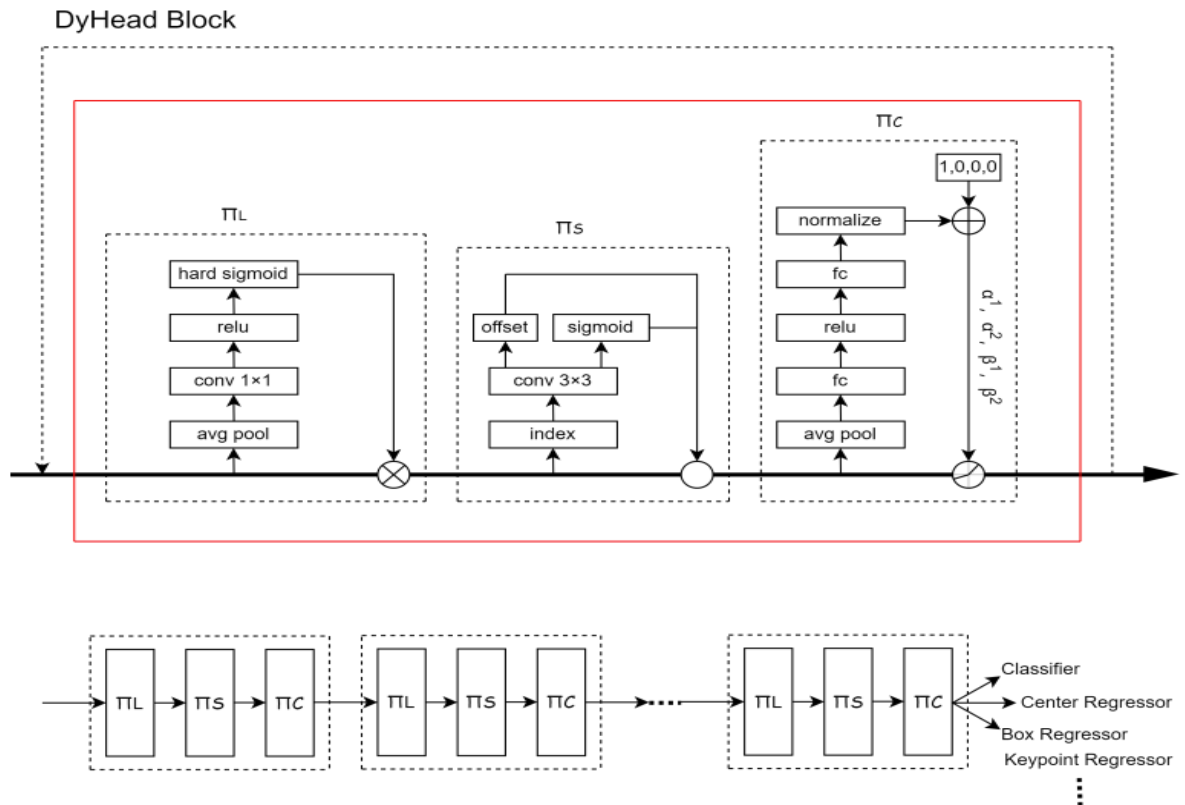


Figure 4. Dynamic Head detailed design network details

2.1.4 YOLOv7-CDD Model

This model adds the CA attention mechanism module to the last layer of all backbone extraction networks in Backbone to replace the original output layer. The detection effect after replacement is better than directly replacing the C3 module of all backbone extraction networks in Backbone with the CA module. It is more accurate and simplified, and does not require manual adjustment of thresholds. And DSCConv was introduced to replace some of the conventional convolutions (3×3 convolution) in

the Backbone Network and some of the conventional convolutions (3×3 convolution) in the multi-branch stacking module Multi_Concat_Block, without reducing the model detection accuracy. Under the premise, the number of parameters of the model can be further reduced. Finally, adding the dynamic detection head Dynamic Head can significantly improve the expression ability of the target detection head without increasing the amount of calculation. The structure of the improved algorithm YOLOv7-CDD network model is shown in Figure 5.

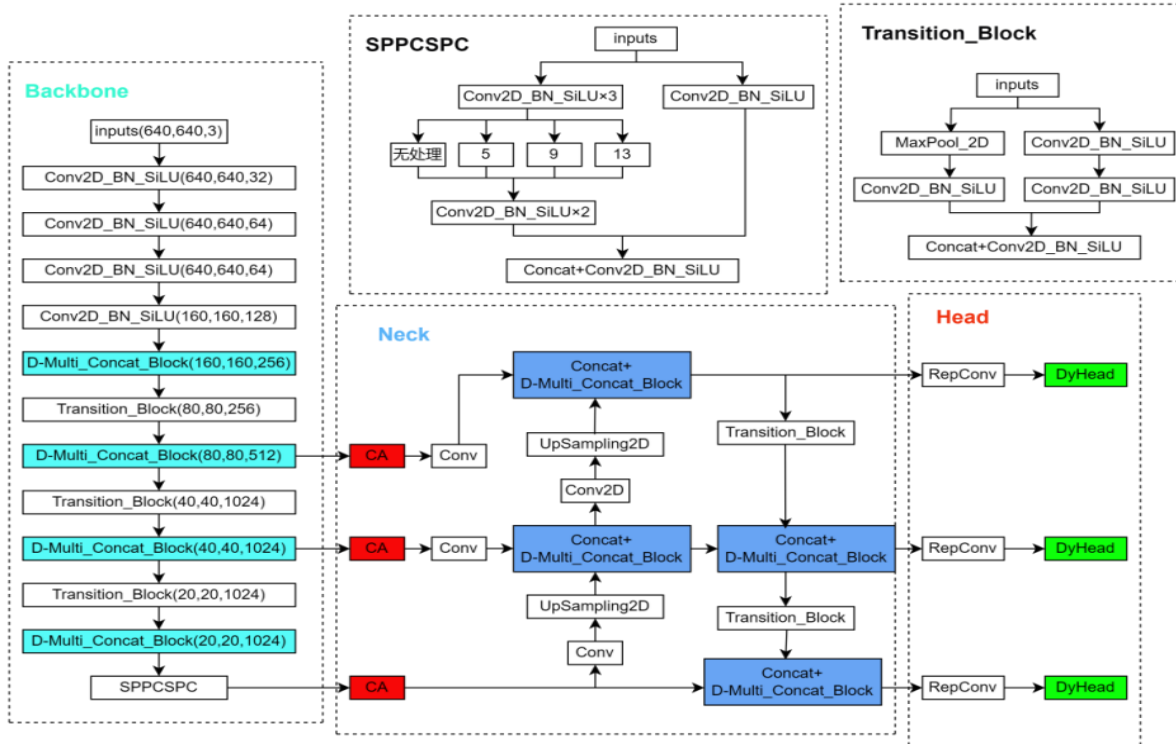


Figure 5. YOLOv7-CDD network model structure

2.2 Experimental Data and Methods

2.2.1 Experimental Environment and Parameter Settings

Experimental environment: The system used in this experiment is Windows 10, Intel(R) Core (TM) i7-9700k-3.6GHz (CPU), NVIDIA-GeForce-RTX-2080Ti-11G*2 (GPU), and 48GB (RAM). The GPU is used to accelerate model training. The software used is PyCharm 2022, CUDA 11.6, Python version 3.8, and the framework is PyTorch version 1.12.0.

Parameter setting: the number of model training iterations is 150, and the batch size is 32.

2.2.2 Dataset

The dataset used in this study is a field scene shot of a ranch in Inner Mongolia, which contains a total of 7166 1280×720 pixel pictures of dairy cows eating and not eating. In the experiment, the ratio of training set, test set and validation set are set to 6:3:1, that is, there are 4300 training set pictures, 2150 test set pictures, and 716 validation set pictures. The data sample is shown in Figure 6.



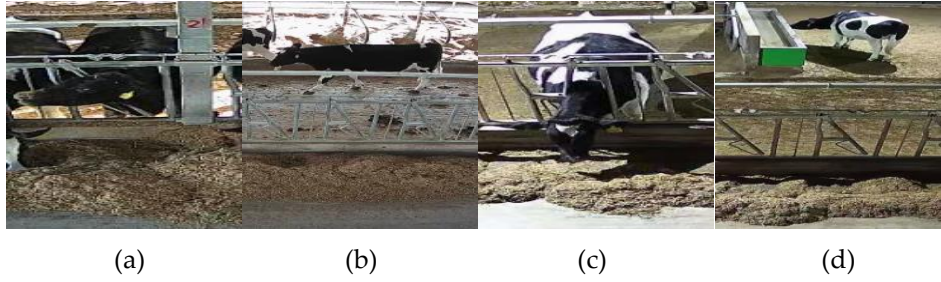


Figure 6. Dairy Cow Feeding Data Set

Note: (a) Eating during the day; (b) not eating during the day; (c) eating at night; (d) not eating at night.

The data annotation software Labeling was used to annotate the cows in the data, and in order to identify the cows' eating behavior, the cows were divided into cow eating (eating cows) and cows (not eating cows). When cows eat, they stick their heads out of the fence to eat. In Figure 5(b), there are two states of cows sticking their heads out of the fence. The left one is eating, and the right one has the desire to eat. For the convenience of the experiment, the cows sticking their heads out of the fence are marked as eating (cow eating). In Figure 5(a), there are three different states of cows. For the convenience of the experiment, they are all marked as not eating cows.

2.2.3 Evaluation Metrics

This experiment uses precision P , recall R , and mean average precision mAP to evaluate the detection efficiency and performance of the YOLOv7-CDD model. The calculation formula is as follows:

$$P = \frac{TP}{TP+FP} \quad (12)$$

$$R = \frac{TP}{TP+FN} \quad (13)$$

$$AP = \int_0^1 P(R)dR \quad (14)$$

$$mAP = \frac{1}{N} \sum_{i=1}^N AP_i \quad (15)$$

Where TP is the number of cows that are correctly predicted to be eating; FP is the number of cows that are incorrectly predicted to be eating; FN is the number of cows that are not predicted to be eating; AP is the average precision of the experiment; N is the number of sample categories.

3. Experimental Results Analysis

3.1 Comparative Experiment on Performance of Different Attention Mechanisms

In order to verify the effectiveness of introducing CA attention mechanism in YOLOv7 in testing the feeding behavior dataset of dairy cows in the pasture, SE attention mechanism, EAM attention mechanism and ECA attention mechanism were used to improve the YOLOv7 model, and the same dataset was tested and compared under the same experimental environment. The comparison results are shown in Table 1.

Table 1. Comparative test of attention mechanisms

Model	P%	R%	mAP%	Parameter quantity	FLOPS/G
YOLOv7	95.6	95.7	96.2	3.721×10^7	1.051×10^{11}
YOLOv7-SE	96.3	96.6	97.1	3.774×10^7	1.023×10^{11}
YOLOv7-EAM	96.9	97.5	97.8	3.842×10^7	1.102×10^{11}
YOLOv7-ECA	96.8	96.7	97.6	3.741×10^7	1.044×10^{11}
YOLOv7-CA	98.3	98.0	98.9	3.715×10^7	1.055×10^{11}

In this m Analysis and comparison results show that after embedding CA attention, the accuracy of the model is 98.3%, which is 2.7%, 2.0%, 1.4%, and 1.5% higher than other models respectively; the recall rate is 98.0%, which is higher than other models. The model improved by 2.3%, 1.4%, 0.5%,

and 1.3% respectively; the average accuracy-to-mean ratio was 98.9%, which was improved by 2.7%, 1.8%, 1.1%, and 1.3% respectively compared with embedding other models; and embedding CA attention. After force, the GFLOPs are larger and the detection speed is

faster. Therefore, the effect of YOLOv7-CA on the model is more significant.

3.2 Ablation Experiment

In order to more comprehensively verify the effectiveness of the three improved methods

proposed in this paper, a series of ablation experiments are carried out in the same experimental environment and experimental equipment. The experimental data are shown in Table 2, and the experimental results are shown in Figure 7.

Table 2. Ablation experiments

Model	P(%)	R(%)	MAP@0.5(%)	Parameter quantity/M	FLOPS/G
YOLOv7	95.6	95.7	96.2	3.721×10^7	1.051×10^{11}
YOLOv7-CA	98.3	98.1	98.9	3.715×10^7	1.055×10^{11}
YOLOv7-DSCConv	98.2	98.1	98.8	3.259×10^7	6.59×10^{10}
YOLOv7-DyHead	98.2	97.7	98.8	3.642×10^7	1.024×10^{11}
YOLOv7-CA+DSCConv	98.1	97.9	98.7	3.274×10^7	6.62×10^{10}
YOLOv7-CA+DyHead	98.1	98.2	98.8	3.657×10^7	1.027×10^{11}
YOLOv7-DSCConv+DyHead	97.8	98.1	98.9	3.642×10^7	6.84×10^{10}
YOLOv7-CDD	98.4	98.3	99.3	3.657×10^7	6.88×10^{10}

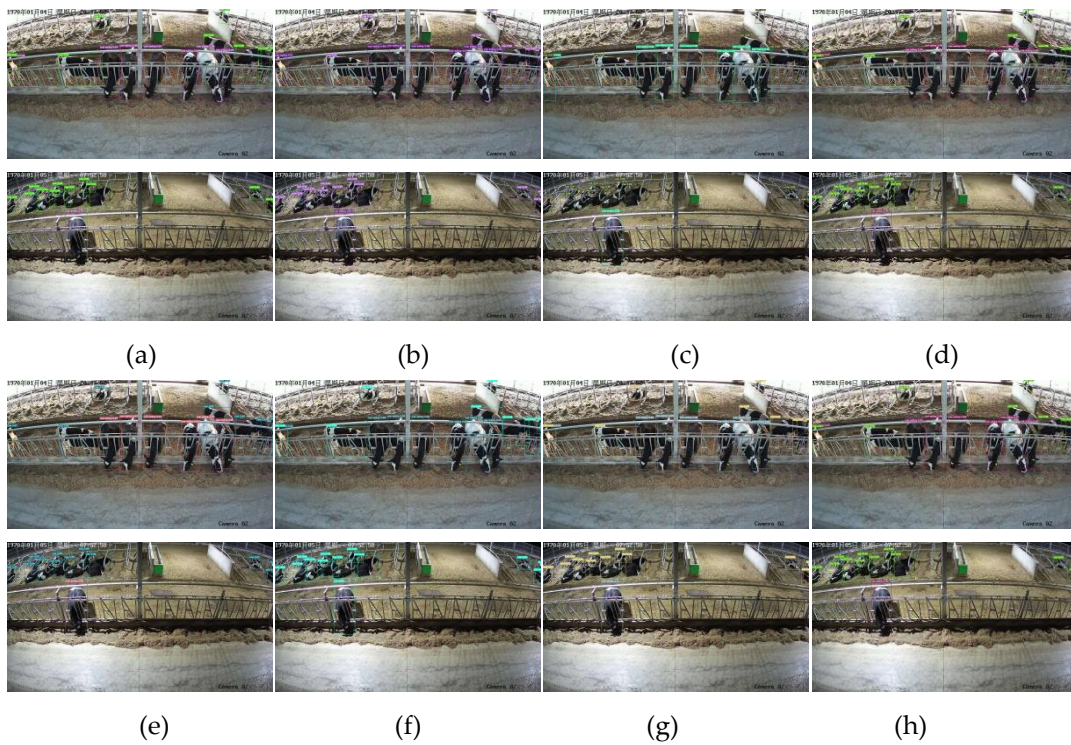


Figure 7. Comparison of detection effects of different algorithms in the same scene

Note: (a) YOLOv7; (b) YOLOv7-CDD; (c) YOLOv7-CA; (d) YOLOv7-DSCConv; (e) YOLOv7-DyHead; (f) YOLOv7-CA+DSCConv; (g) YOLOv7-CA+DyHead; (h) YOLOv7-DSCConv+DyHead.

It can be seen from the above table that the accuracy rate of the original YOLOv7 model is lower than that of other models. After adding the CA attention mechanism based on the YOLOv7 model, Map@0.5 increased by 2.7 percentage points, which improved the accuracy of the

model and slightly reduced the calculation amount, making the model partially lightweight. After adding DSCConv distributed offset convolution, mAP@0.5 increased by 2.6 percentage points and the number of parameters dropped a lot. GFLOPs were significantly

reduced and the calculation amount was slightly reduced. This shows that adding the module can reduce the calculation amount of the model. After adding the Dynamic Head dynamic detection head, the attention mode is systematically considered in the head design to obtain better performance, and mAP@0.5 is increased by 2.6 percentage points. The improved YOLOv7-CDD algorithm increased mAP@0.5 by 3.1 percentage points, and the number of parameters and the number of floating-point operations were significantly reduced, indicating that this algorithm model takes up less memory resources and has better detection performance.

3.3 Comparative Experiment

In order to further verify the objectivity and effectiveness of the improved YOLOv7-CDD network model, different models were compared on the same data set under the same experimental conditions. Under the same configuration environment and training parameters, the comparative experimental results of the improved YOLOv7-CDD network model in this paper and other network models are shown in Table 3.

Table 3. Comparative experiments

Model	P(%)	R(%)	MAP@0.5(%)	Parameter quantity/M	FLOPS/G
YOLOv4	94.3	94.8	95.1	6.313×10^7	6.94×10^{10}
YOLOv5	94.7	94.8	95.4	7.174×10^6	5.99×10^{10}
YOLOv7	95.6	95.7	96.2	3.721×10^7	1.051×10^{11}
YOLOv8	97.9	98.3	99.1	3.006×10^7	8.9×10^{10}
YOLOv7-CDD	98.4	98.3	99.3	3.657×10^7	6.88×10^{10}

From the analysis of Table 3, we can see that the YOLOv7-CDD algorithm proposed in this paper has improved all indicators compared with other algorithms, and the number of parameters and floating-point operations have decreased significantly, and the amount of operations is less than that of other algorithms. The visualization results show that the algorithm proposed in this paper makes the model lighter and the model detection accuracy is improved, and the comprehensive detection effect is better than other algorithms.

4. Conclusion

This paper proposes the YOLOv7-CDD model based on the YOLOv7 target detection model. The model adds the CA attention mechanism and DSCConv distribution offset convolution to make the model lighter, and adds Dynamic Head to the head, which makes the model more accurate in recognizing the behavior of eating cows. The accuracy of the improved model is 98.4%, the recall rate is 98.3%, and the mAP@0.5 is 99.3%, which are all improved compared with the original YOLOv7 model. However, although this improved model is more lightweight, the corresponding FPS will be reduced. In order to better optimize the model, in future research, the

number of FPS frames and the diversification of data sets will be further considered to achieve more innovative research in the recognition of cow eating behavior.

Author Contributions

Conceptualization, W.L. and R.K.; methodology, W.L. and R.K. and Y.Z.; software, R.K; validation, R.K, W.L. and P.Z.; formal analysis, W.L. and R.K.; investigation, R.K; resources, R.K; data curation, R.K; writing – original draft preparation, R.K; writing – review and editing, W.L.; visualization, R.K; supervision, W.L.; project administration, Y.Z.; funding acquisition, W.L. All authors have read and agreed to the published version of the manuscript.

Funding

This research was funded by National Natural Science Foundation of China, NSFC Fund No.62103309.

Institutional Review Board Statement

Not applicable.

Informed Consent Statement

Not applicable.

Data Availability Statement

The dataset cannot be publicly disclosed due to privacy concerns. However, we can provide models and codes. The models and codes that support the findings of this study can be accessed by contacting the corresponding author upon reasonable request.

Conflicts of Interest

The authors declare no conflicts of interest.

Featured Application

This paper can help pasture enterprises or herders to save some costs and make it more convenient for them.

References

- Bai Qiang, Gao Ronghua and Zhao Chunjiang et al. (2022). Multi-scale behavior recognition method of dairy cows based on improved YOLOV5s network. *Transactions of the Chinese Society of Agricultural Engineering*, 38(12), 163-172.
- Cui Liqun, Cao Huawei. (2024, May). Improved YOLOv7 for aerial image target detection. *Computer Engineering and Applications*, 1-11.
- Deng Changzheng, Liu Mingze and Fu Tian et al. (2024, March). Infrared image recognition of substation equipment based on improved YOLOv7-Tiny. *Infrared Technology*, 1-8.
- Eleonora F, Alberto R and Mirco C et al. (2023). Eating time of dairy cows: a study focusing on commercial farms. *Italian Journal of Animal Science*, 22(1), 1023-1032.
- Jia Xueying, Zhao Chunjiang and Zhou Juan et al. (2023). Online detection of citrus surface defects based on improved YOLOv7 model. *Transactions of the Chinese Society of Agricultural Engineering*, 39(23), 142-151.
- Li Yuwei, Fu Rui and Liu Fan. (2024). Improved YOLOv7 lightweight traffic sign detection algorithm. *Journal of Taiyuan University of Technology*, 55(01), 195-203. DOI: 10.16355/j.tyut.1007-9432.2023BD009.
- Li Z, Zhu Y and Sui S et al. (2024). Real-time detection and counting of wheat ears based on improved YOLOv7. *Computers and Electronics in Agriculture*, 218, 108670.
- Liu Yuefeng, Bian Haodong and He Yingjie et al. (2022). Multi-target dairy cow eating behavior recognition method based on amplitude iterative pruning. *Transactions of the Chinese Society of Agricultural Machinery*, 53(02), 274-281.
- Niu Weihua, Wei Yali. (2024). Aerial small target detection algorithm based on improved YOLOv 7. *Electro-Optics & Control*, 31(01), 117-122.
- Qin Lifeng, Zhang Xiaoqian and Dong Mingxing et al. (2021). Moving cow target extraction based on multi-feature fusion correlation filtering. *Transactions of the Chinese Society of Agricultural Machinery*, 52(11), 244-252.
- Qu Chenyang, Cheng Yanyun. (2024, January). Traffic sign detection algorithm based on improved YOLOv7. *Microelectronics and Computers*, 1-11.
- Song Huaibo, Li Rong and Wang Yunfei et al. (2023). Severely occluded beef cattle target recognition method based on ECA-YOLO v5s network. *Transactions of the Chinese Society of Agricultural Machinery*, 54(03), 274-281.
- Song Lvming, Liu Mingqin and Li Xiangbin et al. (2024, January) Research on glass surface defect detection method based on improved YOLOv7. *Mechanical and Electrical Engineering Technology*, 1-10.
- Wang Zheng, Xu Xingshi and Hua Zhixin et al. (2022). Lightweight dairy cow estrus behavior recognition based on YOLOv5n and channel pruning algorithm. *Transactions of the Chinese Society of Agricultural Engineering*, 38(23), 130-140.
- Xing Yongxin, Sun Youdong and Wang Tianyi. (2022). Individual recognition of dairy cows based on improved SSD algorithm. *Computer Engineering and Applications*, 58(02), 208-214.
- Xu Hongwei, Li Ran and Zhang Jiaxu. (2024). Lake floating object detection algorithm based on improved YOLOv7. *Modern Electronic Technology*, 47(01), 105-110. DOI: 10.16652/j.issn.1004-373x.2024.01.019.
- Xu Ming, Qu Taipeng and Jiang Yanji. (2024, May). Improved YOLOv7 traffic sign detection algorithm in complex scenes. *Computer Engineering*, 1-11.
- Zhang Zhen, Zhou Jun and Jiang Zizhen et al. (2024) Apple recognition method in natural orchard environment based on improved YOLO v7 lightweight model. *Transactions of the Chinese Society of Agricultural Machinery*, 55(03), 231-242+262.

Zou J, Arshad RM. (2024). Detection of whole body bone fractures based on improved YOLOv7. *Biomedical Signal Processing and Control*, 91, 105995.

MPPT Techniques in Wind-Solar Hybrid Systems: A Review of Algorithms and Implementation

Wei Liang¹

¹ Guangxi University of Science and Technology, Liuzhou, China

Correspondence: Wei Liang, Guangxi University of Science and Technology, Liuzhou, China.

doi:10.56397/JPEPS.2025.04.06

Abstract

The increasing global demand for sustainable and decentralized energy solutions has accelerated the adoption of wind-solar hybrid renewable energy systems. These systems offer improved reliability and energy availability by leveraging the complementary nature of solar and wind resources. However, the inherent variability and nonlinear characteristics of these sources necessitate the use of Maximum Power Point Tracking techniques to ensure optimal power extraction under changing environmental conditions. This paper presents a comprehensive review of both classical and intelligent MPPT algorithms, including Perturb and Observe, Incremental Conductance, Fuzzy Logic Control, Artificial Neural Networks, Particle Swarm Optimization, and hybrid approaches. The paper critically examines the principles, implementation strategies, strengths, and limitations of each method, with a focus on their application in wind-solar hybrid systems. Particular attention is given to the integration challenges associated with real-time deployment, control coordination between energy sources, convergence stability, and computational overhead. Emerging trends such as IoT-enabled control, machine learning integration, and predictive optimization are also discussed. This review aims to guide researchers and system designers in selecting and developing MPPT strategies that balance efficiency, adaptability, and system complexity for future-ready hybrid renewable energy applications.

Keywords: wind-solar hybrid systems, maximum power point tracking, perturb and observe, incremental conductance, artificial neural networks, particle swarm optimization

1. Introduction

As the global energy landscape continues to shift toward sustainable and decentralized power generation, hybrid renewable energy systems have gained significant attention as a practical and efficient solution to meet growing energy demands while minimizing environmental impacts. Among various combinations of renewable sources, wind-solar hybrid systems stand out due to the

complementary nature of solar irradiance and wind patterns. Typically, solar power peaks during sunny, clear days, while wind energy can be harnessed both during the day and night and in conditions where solar resources may be limited. This synergy enhances system reliability and energy yield, particularly in remote or off-grid areas where consistent power supply is critical.

Despite their advantages, wind-solar hybrid

systems present unique operational and technical challenges. One of the most prominent among them is the dynamic and intermittent behavior of the energy inputs—solar irradiance and wind speed—which directly affect the efficiency of energy conversion and utilization. The inherent non-linear characteristics of photovoltaic panels and wind turbines require sophisticated control mechanisms to ensure optimal performance. Without proper management, these systems risk underperformance, energy losses, and reduced economic viability.

To address these issues, Maximum Power Point Tracking techniques have become a cornerstone in the control strategy of hybrid energy systems. MPPT algorithms continuously monitor and adjust the operating points of the PV panels and wind turbines to ensure that they operate at their respective maximum power points under varying environmental conditions. This adaptive capability significantly improves energy harvest and enhances overall system efficiency.

The implementation of MPPT in hybrid systems is particularly challenging compared to standalone PV or wind systems. This is due to the need for coordinated control of two disparate energy sources, each with its own set of variables and response characteristics. The presence of power electronics—such as DC-DC converters and inverters—further complicates the system dynamics, requiring real-time, robust, and efficient MPPT strategies. The integration of battery storage systems adds another layer of complexity, especially when MPPT must consider load variations and storage capacity in real time.

Recent advancements in computational intelligence and control algorithms have led to the development of sophisticated MPPT methods, ranging from classical approaches like Perturb and Observe and Incremental Conductance to more advanced techniques including fuzzy logic controllers, artificial neural networks, particle swarm optimization, and hybrid algorithms that blend multiple strategies. These innovations aim to improve the speed of convergence, reduce power oscillations, and adapt to rapidly changing environmental conditions with minimal energy losses.

The increasing role of digital technologies—such as the Internet of Things, machine learning, and real-time analytics—in the energy sector is

paving the way for smarter MPPT implementations. These technologies enable predictive control, remote monitoring, and decentralized decision-making, all of which contribute to a more resilient and efficient hybrid energy infrastructure.

In this context, a comprehensive understanding of MPPT techniques and their implementation in wind-solar hybrid systems is essential for researchers, engineers, and policymakers aiming to optimize renewable energy utilization. This review explores the evolution of MPPT algorithms, their comparative performance, real-world implementation challenges, and future directions in the context of hybrid renewable energy systems.

2. Overview of MPPT in Hybrid Systems

Maximum Power Point Tracking lies at the heart of operational efficiency in wind-solar hybrid renewable energy systems. These systems harness energy from two inherently distinct sources—solar photovoltaic modules and wind turbines—each subject to nonlinear output behaviors that are driven by independent and highly variable environmental factors. The dynamic nature of these input variables necessitates sophisticated control algorithms to continuously extract the maximum available power from both sources under all operating conditions.

In PV systems, the maximum power point shifts according to changes in solar irradiance, ambient and cell temperature, and shading conditions. This creates a power-voltage curve with a single peak, which must be tracked continuously to maximize efficiency. Wind energy systems, on the other hand, exhibit a more complex relationship between output power and input conditions. The wind turbine's power output is influenced not only by wind speed but also by turbine design parameters such as blade pitch, swept area, tip speed ratio, and generator characteristics. This results in a power curve that often contains multiple operating points depending on the control method (e.g., fixed speed vs. variable speed operation), making MPPT in wind systems inherently more complex than in PV systems.

In a hybrid system where both PV and wind subsystems are integrated, the task of MPPT becomes multifaceted. Solar and wind sources exhibit asynchronous behavior—not only do they peak at different times of day or under

different weather conditions, but they also vary in their response speed to environmental stimuli. For instance, solar irradiance may rise and fall gradually due to cloud cover, whereas wind speed can change suddenly due to turbulence. These variations necessitate real-time monitoring and dual-source optimization to ensure that each energy source operates at or near its MPP while minimizing energy loss through mismatch or overload.

The coordination of energy extraction from both sources often involves advanced power electronic interfaces, such as individual or multi-input DC-DC converters, coupled to a shared DC bus. In this configuration, the MPPT algorithm must manage the operating point of each input channel without destabilizing the overall system. This is further complicated when storage devices such as batteries or supercapacitors are introduced, requiring dynamic regulation of charge/discharge rates to maintain system balance and extend component life. Hybrid inverters, capable of managing inputs from both wind and solar sources, must also integrate MPPT control loops to ensure efficient AC output generation while synchronizing with grid or load requirements.

Beyond energy extraction, MPPT also plays a crucial role in system-wide performance. Efficient MPPT enhances total energy yield by keeping subsystems at their optimal power-producing states, which reduces the need for oversizing and contributes to more compact, cost-effective designs. Real-time MPPT contributes to operational stability by minimizing power oscillations and reducing the stress on power electronic components. It also ensures that fluctuations in source power do not destabilize the DC-link voltage or induce harmonic distortion in the AC output, which is especially critical in grid-tied and microgrid applications.

Modern MPPT strategies are increasingly incorporating elements of artificial intelligence, adaptive control, and predictive modeling. Techniques such as machine learning-based prediction, fuzzy logic control, and reinforcement learning are being integrated into MPPT frameworks to enable context-aware decision-making, self-tuning of control parameters, and learning from historical performance patterns. These capabilities are especially useful in complex operating scenarios, such as those involving partial shading in PV

arrays, gusty wind conditions, or non-linear storage dynamics. AI-driven MPPT can also anticipate environmental changes based on forecasting data, enabling proactive rather than reactive optimization.

These trends reflect a broader shift from rigid, rule-based control systems toward autonomous, data-driven control architectures capable of adapting to the diverse and evolving conditions typical of hybrid renewable energy deployment. This evolution is critical not only for maximizing the immediate power output but also for ensuring long-term system resilience, reducing maintenance costs, and supporting the integration of HRES into smart grids, electric vehicle charging networks, and other advanced energy infrastructures.

In conclusion, MPPT in wind-solar hybrid systems is far more than a passive optimization tool—it is the cognitive layer of modern renewable energy systems. As these systems scale in both size and sophistication, the role of MPPT will expand further, demanding algorithms that are not only efficient and accurate but also intelligent, resilient, and capable of operating in real-world, dynamic environments. Future MPPT research and implementation must continue to bridge control theory, data science, and embedded systems design to meet the energy challenges of a low-carbon, distributed energy future.

3. Classical and Intelligent MPPT Techniques

Maximum Power Point Tracking algorithms are at the core of ensuring that hybrid renewable energy systems extract the maximum possible power from their sources at any given moment. In wind-solar hybrid systems, where the power output characteristics of each source are nonlinear and vary independently, the role of MPPT becomes even more critical. Over the years, MPPT methodologies have evolved from simple, reactive techniques into sophisticated, predictive, and adaptive control systems. This evolution reflects not only the increasing demand for energy optimization under diverse and uncertain environmental conditions but also the rapid advancement in embedded processing, digital control systems, and artificial intelligence.

Classical MPPT techniques have been widely implemented in commercial and academic projects due to their simplicity, ease of integration, and minimal computational

demand. Among the most prominent classical methods are Perturb and Observe and Incremental Conductance. The P&O algorithm functions by slightly perturbing the operating voltage or current of a PV module or wind generator and observing the resulting change in output power. If the power increases, the system continues to perturb in the same direction; otherwise, it reverses the direction of perturbation. Although effective under stable conditions, P&O struggles with rapid environmental changes. It can oscillate around the MPP, especially in steady-state conditions, leading to minor but persistent energy losses. More critically, during fast-changing irradiance or wind speed, P&O can be misled into tracking the wrong direction, resulting in substantial deviations from the optimal operating point.

The Incremental Conductance method attempts to overcome this by comparing the rate of change in current (dI) to the rate of change in voltage (dV). When dI/dV equals $-I/V$, the system is theoretically operating at its MPP. This technique allows for more accurate tracking during transient conditions, particularly in solar systems, and performs better than P&O when irradiance changes are gradual. However, IC methods still rely on real-time differentiation, which introduces sensitivity to measurement noise and requires precise analog-to-digital conversion. This can be challenging in embedded systems with limited resolution, especially when deployed in harsh field conditions with fluctuating temperature and electromagnetic interference.

Given these limitations, research has increasingly turned toward intelligent MPPT algorithms that leverage heuristic, adaptive, and bio-inspired approaches. These techniques offer enhanced flexibility, noise tolerance, and real-time learning capabilities. Fuzzy Logic Control is one of the earliest intelligent techniques adapted for MPPT. It uses a rule-based inference system to process inputs such as the change in power and voltage to determine the next operating point. FLC does not require an explicit mathematical model of the system and can operate effectively under imprecise, noisy, or incomplete data conditions. Its adaptability and fast response make it especially useful in environments where input parameters change unpredictably, such as wind-solar systems with cloud-induced variability or gusty winds.

Artificial Neural Networks represent a paradigm shift in MPPT control. Trained using historical and simulated data, ANNs are capable of identifying complex nonlinear relationships between environmental conditions (e.g., irradiance, wind speed, temperature) and the corresponding maximum power points. Once trained, ANNs can infer the optimal operating point almost instantaneously, providing extremely fast tracking with minimal oscillation. However, their implementation presents several challenges. The accuracy of an ANN depends heavily on the quality and comprehensiveness of the training data. Neural networks are computationally intensive and memory-demanding, which may preclude their use in small-scale embedded controllers unless paired with specialized hardware like FPGAs or AI co-processors.

Particle Swarm Optimization offers another intelligent solution by treating MPPT as a multidimensional optimization problem. Each "particle" in the swarm represents a candidate solution, and particles adjust their positions in the search space based on their own experience and that of neighboring particles. This approach excels in complex and multimodal search spaces, such as those encountered in partially shaded PV arrays or nonlinear wind turbine response curves. PSO is inherently parallelizable and robust to local maxima, but it requires careful tuning of parameters such as inertia weight and acceleration coefficients to balance exploration and convergence speed. PSO's convergence time can be slower than that of model-free methods under rapidly changing input conditions, unless paired with predictive enhancements or hybridized with faster algorithms.

In response to the trade-offs between performance and complexity, hybrid MPPT algorithms have been proposed to combine the strengths of both classical and intelligent methods. For example, a system might employ P&O under stable weather conditions to conserve computational resources, while dynamically switching to an ANN or FLC controller during high variability. Some systems use ANNs to generate initial conditions for PSO or GA (Genetic Algorithm) searches, accelerating convergence. Others utilize fuzzy logic to modulate the perturbation size in P&O, thereby reducing oscillations without sacrificing simplicity. These hybrid systems provide a balance between robustness, speed, and

implementability, making them increasingly attractive for real-world deployments in hybrid energy systems.

As these intelligent MPPT strategies continue to mature, their integration into smart energy systems is becoming more seamless through the use of IoT, edge computing, and real-time analytics. IoT-enabled MPPT controllers can collect and transmit environmental and operational data for centralized learning or predictive modeling. Edge devices can host lightweight AI algorithms that continuously adapt to localized conditions, enabling distributed decision-making and fault tolerance. Predictive analytics, driven by weather forecasts and load trends, can also feed into MPPT systems to preemptively adjust operating points, minimizing energy losses during known environmental transitions.

In conclusion, while classical MPPT techniques remain valuable for their simplicity, proven reliability, and ease of deployment, the future of MPPT lies in the intelligent orchestration of advanced control techniques. Intelligent and hybrid MPPT algorithms not only provide better performance in complex and fast-changing environments but also align with the broader vision of autonomous, adaptive, and efficient renewable energy systems. As embedded hardware becomes more powerful and accessible, and as smart grid infrastructure evolves, the widespread adoption of intelligent MPPT will become both feasible and necessary for the next generation of sustainable energy systems.

4. Algorithmic Integration in Hybrid Systems

The integration of Maximum Power Point Tracking (MPPT) algorithms into wind-solar hybrid renewable energy systems (HRES) is not merely a technical optimization challenge—it represents a complex systems engineering problem. It requires the co-design of power electronics, embedded control software, and energy management strategies to harmonize two fundamentally dissimilar and independently fluctuating energy sources. Unlike single-source PV or wind systems, hybrid configurations must accommodate solar irradiance and wind velocity, which are uncorrelated in their temporal and spatial variations. This makes the optimization task multidimensional, with intertwined objectives such as real-time tracking, power balancing, storage control, and load matching.

One widely adopted approach to MPPT deployment in hybrid systems is the decoupled control strategy, wherein solar and wind modules are treated as independent energy subsystems, each with dedicated converters and MPPT logic. This modular approach offers implementation flexibility and scalability. For instance, solar modules typically use Perturb and Observe (P&O) or Incremental Conductance (IC) algorithms, given their predictable P–V characteristics. Wind systems, however, are better suited to algorithms like Tip Speed Ratio (TSR), Power Signal Feedback (PSF), or Optimal Torque Control, which consider the turbine’s mechanical properties and nonlinear aerodynamic responses. As emphasized by Kumar and Chatterjee, the effectiveness of wind MPPT is highly contingent on site-specific turbine parameters such as rotor diameter, generator inertia, and air density—necessitating algorithm tuning or adaptation for each deployment environment.

In more integrated architectures—particularly those involving a common DC bus or hybrid inverter—a centralized or coordinated MPPT strategy becomes necessary. This adds considerable complexity, as the MPPT controller must not only optimize each input stream but also orchestrate system-wide operations such as source prioritization, dynamic load sharing, and coordinated energy dispatch. For example, during midday hours, solar output may exceed immediate consumption while wind power remains constant. The system controller must decide whether to prioritize storing excess solar power, curtail it, or allow wind to supplement the load depending on battery state-of-charge (SoC), load demand patterns, and converter capacity. Real-time optimization under such constraints demands high-speed decision-making, fault tolerance, and predictive adaptability.

To meet these demands, researchers have increasingly turned to metaheuristic optimization algorithms and soft computing approaches that offer flexible, real-time adaptability in complex decision spaces. Among these, Genetic Algorithms (GAs) are popular for their robustness in exploring global solution spaces. GAs apply principles of natural selection—mutation, crossover, and elitism—to evolve optimal controller parameters for MPPT in varying environmental contexts. For example, GA-based MPPT can fine-tune DC-DC converter

duty cycles or wind turbine control parameters based on historical irradiance and wind profiles, thus maximizing efficiency while avoiding oscillatory behavior.

Adaptive Neuro-Fuzzy Inference Systems (ANFIS) represent another powerful class of intelligent MPPT tools. Combining the human-like reasoning of fuzzy logic with the learning capabilities of neural networks, ANFIS systems dynamically refine their rule base through exposure to operational data. This makes them particularly well-suited for hybrid systems operating in non-ideal conditions, such as partial shading in PV arrays or wind turbulence. Unlike static rule-based systems, ANFIS can self-improve over time, adjusting to aging components, seasonal changes, and altered load profiles.

Particle Swarm Optimization (PSO), inspired by collective behavior in natural systems, has also been successfully applied in hybrid MPPT scenarios. PSO's strength lies in its balance between local search and global exploration, allowing it to escape local maxima—a common problem in MPPT under complex energy landscapes. For instance, in systems subject to partial shading or gusty winds, PSO can converge on the true global maximum with fewer iterations than exhaustive search-based methods.

Roy et al. highlight the multi-objective optimization capabilities of these intelligent methods, which not only maximize power extraction but also stabilize voltage, minimize harmonic distortion, regulate battery health, and ensure compliance with grid codes. These algorithms are robust to sensor noise, measurement error, and component degradation—making them well-suited for real-world deployments.

The integration of energy storage systems (ESS) such as lithium-ion batteries or supercapacitors introduces another layer of control complexity. MPPT algorithms must now be integrated into a larger energy management system (EMS), where real-time decisions account for battery SoC, charge-discharge efficiency, and thermal constraints. In these cases, hierarchical control architectures are often used. The lower layer comprises fast-acting MPPT controllers that optimize individual sources, while upper-level supervisory controllers manage system-wide objectives such as storage scheduling, peak

shaving, and grid export control. Techniques like Model Predictive Control (MPC), which use system models to forecast future states, are increasingly deployed at this level to support predictive and proactive decision-making.

As hybrid systems move toward microgrid integration, distributed control becomes a crucial requirement. Multi-agent systems (MAS), where autonomous agents (e.g., wind MPPT, solar MPPT, battery controller) communicate and collaborate, are gaining traction for decentralized, fault-resilient control. Each agent can locally optimize its subsystem while contributing to global objectives like frequency regulation, cost minimization, or energy trading.

To validate and refine such complex control schemes, hardware-in-the-loop (HIL) testing and real-time simulation platforms have become indispensable. These tools simulate hybrid energy environments in real time, enabling developers to test MPPT performance across diverse scenarios including variable weather, load transients, or communication failures. This not only accelerates algorithm development but also ensures safety and reliability before field deployment.

In conclusion, algorithmic integration of MPPT in hybrid wind-solar systems is evolving from simple, source-specific optimization to a holistic, system-level coordination challenge. As energy systems grow more interconnected, intelligent MPPT must adapt to increasingly dynamic environments, interface seamlessly with storage and grid assets, and operate autonomously under a wide range of uncertainties. Future advancements will likely come from the intersection of artificial intelligence, power electronics, and distributed control, forming the foundation for resilient and intelligent renewable energy systems.

5. Implementation Challenges and Future Directions

Despite their theoretical promise and growing adoption, the practical implementation of advanced Maximum Power Point Tracking algorithms in wind-solar hybrid energy systems remains fraught with significant technical and systemic challenges. One of the most pressing issues is the computational burden posed by intelligent MPPT algorithms. Techniques like Particle Swarm Optimization, Artificial Neural Networks, and Adaptive Neuro-Fuzzy Inference Systems require complex calculations, iterative

processes, or large datasets for training. These algorithms, while accurate and adaptable, are often unsuitable for real-time implementation on low-cost microcontrollers or digital signal processors with limited processing power and memory. In field applications, particularly in remote or off-grid locations, power electronics controllers are usually designed for minimal energy consumption and maximum reliability, and embedding computationally heavy algorithms into such systems may lead to performance bottlenecks, slower response times, and increased costs.

In addition to computational load, sensor dependency poses another major obstacle. Advanced MPPT algorithms typically require continuous feedback of system parameters such as voltage, current, temperature, irradiance, and wind speed. These sensors are vulnerable to noise, calibration drift, aging, and environmental damage from dust, moisture, or temperature extremes. Sensor faults or inaccurate measurements can significantly distort the algorithm's perception of the system's state, resulting in suboptimal tracking, increased switching activity, or even hardware stress. This dependence on accurate sensing necessitates robust filtering and diagnostic methods, which in turn add to the algorithmic and system complexity.

Stability is another persistent concern. In hybrid systems, the interaction between solar and wind power sources—each governed by distinct, nonlinear characteristics—can lead to complex system behavior. Oscillations around the maximum power point, hunting phenomena due to overcorrection, and erratic behavior under rapidly changing environmental conditions are commonly observed when classical algorithms like Perturb and Observe are used. Even intelligent methods, if not well tuned or trained for specific site conditions, can lead to instability, especially during partial shading in PV arrays or turbulent wind events. Hybrid energy systems further complicate this with power-sharing coordination, load balancing, and battery management, all of which impose additional constraints that the MPPT controller must respect without destabilizing the system.

Another significant challenge is the convergence speed of the MPPT algorithm. In real-world conditions where solar irradiance may change rapidly due to moving clouds or where wind speed fluctuates irregularly, an MPPT algorithm

must track the new maximum point quickly and accurately. Slow convergence not only reduces harvested energy but also risks prolonged mismatch between generated power and load or storage requirements. Faster algorithms, on the other hand, often increase switching frequency, which can elevate system losses, create electromagnetic interference, and shorten the lifespan of power electronic components.

The presence of multiple local maxima—especially in scenarios like partial shading for PV systems or in wind turbines operating across nonlinear aerodynamic zones—poses a significant hurdle. Many traditional MPPT techniques are designed for single-peak curves and can become trapped in local maxima, leading to long-term inefficiencies. Ensuring that an algorithm can distinguish between local and global maxima under all environmental conditions requires additional logic, exploration mechanisms, or predictive capabilities, which can add substantial overhead.

In hybrid systems that incorporate energy storage—such as batteries or supercapacitors—the MPPT algorithm must also consider the real-time status of these elements, including state of charge, charge/discharge limits, aging, and thermal behavior. Failing to incorporate these parameters can lead to overcharging, deep discharging, or cycling inefficiencies that degrade battery life. The MPPT controller must thus be integrated with energy management strategies, which increases software complexity and requires accurate models of battery behavior.

The structural design of the control architecture also poses challenges. Designers must choose between decentralized MPPT control—where each energy source operates its own algorithm—and centralized MPPT, where a master controller orchestrates energy flow among multiple sources. Each approach has trade-offs: decentralized systems can suffer from coordination issues and conflicting control actions, while centralized systems require extensive real-time data exchange and tight synchronization between subsystems.

These challenges highlight the need for more resilient, fault-tolerant, and adaptive MPPT designs, particularly as hybrid systems become more complex and are deployed in diverse environments. Future directions are increasingly

shaped by the integration of emerging technologies such as embedded machine learning, Internet of Things connectivity, and edge computing. These innovations are enabling smarter MPPT algorithms capable of learning from past behavior, predicting future energy availability, and making context-aware decisions. Model predictive control and multi-agent architectures are beginning to be explored for their ability to manage distributed control tasks across hybrid systems and microgrids, offering a promising path toward more autonomous and robust renewable energy management.

6. Conclusion

Maximum Power Point Tracking techniques are fundamental to the optimal operation and energy harvesting of wind-solar hybrid renewable energy systems. As global energy systems pivot toward sustainability, decentralization, and intelligent control, the efficiency and resilience of hybrid energy systems increasingly hinge on the performance of MPPT algorithms. These algorithms ensure that photovoltaic arrays and wind turbines—each subject to different and highly variable environmental inputs—continuously operate at their most efficient points, maximizing power output, minimizing energy loss, and enhancing the overall stability of the system.

Classical MPPT methods such as Perturb and Observe and Incremental Conductance have laid the groundwork for real-time control due to their ease of implementation, minimal computational requirements, and sufficient performance under stable environmental conditions. However, their inherent limitations—particularly oscillatory behavior near the maximum power point, poor performance under rapidly fluctuating inputs, and susceptibility to local maxima—have exposed the need for more sophisticated solutions.

To address these limitations, intelligent MPPT techniques have emerged as a powerful class of solutions. Methods such as Fuzzy Logic Control, Artificial Neural Networks, Particle Swarm Optimization, and Adaptive Neuro-Fuzzy Inference Systems provide superior adaptability, faster dynamic response, and the ability to operate under noisy or incomplete data conditions. These algorithms are especially well-suited for the nonlinear and coupled

dynamics present in hybrid systems where solar and wind inputs may interact in complex ways. Hybrid algorithms that combine classical and intelligent methods are increasingly being adopted to strike a balance between performance, complexity, and real-time feasibility.

Despite their advantages, the deployment of advanced MPPT techniques in practical systems is still confronted by numerous challenges, including computational load, sensor dependency, convergence issues, and stability under highly dynamic conditions. These issues are further compounded in large-scale or off-grid systems where resource constraints, communication delays, and hardware limitations must also be considered. In addition, the integration of energy storage elements and coordination with demand-side management and grid interaction protocols further elevates the importance of robust and adaptive MPPT control.

The evolution of MPPT will likely be shaped by the convergence of multiple technological trends. The incorporation of embedded machine learning and edge computing capabilities is expected to enable low-power, intelligent controllers that can learn from operational data and make context-aware decisions in real-time. Predictive control models and digital twins may also become integral, allowing systems to forecast environmental conditions and proactively adjust power flows. The expansion of Internet of Things platforms will allow MPPT systems to participate in broader energy management frameworks, enabling interoperability with smart grids, microgrids, and distributed energy markets.

Future research should thus prioritize the development of lightweight, scalable, and adaptive MPPT algorithms that are not only computationally efficient but also robust under a wide range of operating scenarios. These next-generation algorithms must seamlessly integrate data-driven intelligence, forecast-based control, and hierarchical energy management strategies to ensure that wind-solar hybrid systems can reliably and autonomously meet the energy demands of a sustainable future.

References

- Bollipo, R. B., & Mikkili, S. (2020). Hybrid, optimal, intelligent and classical PV MPPT techniques: A review. *IEEE Access*. Retrieved

from

<https://ieeexplore.ieee.org/abstract/document/9171659/>

- Chandra, S., Gaur, P., & Srishti. (2018). Maximum power point tracking approaches for wind–solar hybrid renewable energy system—A review. In *Soft Computing: Theories and Applications* (pp. 3–13). Springer. Retrieved from https://link.springer.com/chapter/10.1007/978-981-13-0662-4_1
- Kabalci, E. (2013). Design and analysis of a hybrid renewable energy plant with solar and wind power. *Energy Conversion and Management*, 72, 51–59. Retrieved from <https://www.sciencedirect.com/science/article/pii/S0196890413001271>
- Kumar, D., & Chatterjee, K. (2016). A review of conventional and advanced MPPT algorithms for wind energy systems. *Renewable and Sustainable Energy Reviews*, 55, 957–970. Retrieved from <https://www.sciencedirect.com/science/article/pii/S1364032115012654>
- Kumar, G. B. A., & Shivashankar. (2022). Optimal power point tracking of solar and wind energy in a hybrid wind solar energy system. *Environmental Science and Pollution Research*. Retrieved from <https://link.springer.com/article/10.1007/s40095-021-00399-9>
- Roy, P., He, J., Zhao, T., & Singh, Y. V. (2022). Recent advances of wind-solar hybrid renewable energy systems for power generation: A review. *IEEE Access*. Retrieved from <https://ieeexplore.ieee.org/abstract/document/9684974/>